# Energy & Environmental Science



**REVIEW** 

View Article Online



Cite this: DOI: 10.1039/c8ee03559h

# Chemical stability and instability of inorganic halide perovskites

Yuanyuan Zhou \*\* and Yixin Zhao \*\*\*

Inorganic halide perovskites (IHPs) have recently attracted huge attention in the field of optoelectronics. IHPs are generally expected to exhibit superior chemical stability over the prevailing hybrid organic—inorganic perovskites that are widely used in optoelectronic devices such as solar cells and light-emitting devices. This is primarily owing to the elimination of weakly-bonded organic components in the IHP crystal structure. Nevertheless, many recent studies have revealed that IHPs still suffer significant issues in chemical instability, and thus, a lot of effort has been made towards the stabilization of IHPs for high-performance devices. In this context, a great deal of interest in the chemistry and perovskite community has been emerging to understand the chemical (in)stability of IHPs and develop engineering strategies for making more robust perovskite devices. This review will summarize the past research progress in this direction, give insights into the IHP (in)stability, and provide perspectives for the future effort in making stable IHP materials and devices.

Received 6th December 2018, Accepted 20th February 2019

DOI: 10.1039/c8ee03559h

rsc.li/ees

#### **Broader context**

Halide perovskites (HPs) are a family of new-generation semiconductor materials, which are broadly divided into two types, hybrid organic-inorganic HPs and inorganic HPs. While hybrid HPs have attracted huge attention for application in various (opto)electronics such as solar cells, light-emitting devices, radiation/photo detectors, scintillators, transistors, and memristors, inorganic HPs are also emerging as an intrinsically or thermally more stable alternative to hybrid HPs. Regardless of the promise, inorganic HPs still undergo degradation, which affects the device performance significantly. Therefore, there is an urgent need to gain insights into the chemical stability and instability in inorganic HPs, which will help the development of high-performance perovskite (opto)electronic devices that are sufficiently durable for real-world applications. The chemistry and materials science emerging from the study of inorganic HPs may have a long-lasting impact on other materials with similar behaviors.

#### 1. Introduction

In recent years, halide perovskites have emerged as a new generation of semiconducting materials that are catalyzing a revolution in the field of optoelectronics.<sup>1–7</sup> These halide perovskite materials are not only easy to synthesize by using a variety of solution-/vapor-based methods, but also exhibit outstanding optoelectronic properties such as long carrier diffusion-lengths, moderate carrier mobility, high light-absorption coefficients, and tunable optical bandgaps.<sup>8–10</sup> Halide perovskites are also exceptional for their intrinsic tolerance to defects as the defect states in these materials are usually within the valence and

$$t = \frac{r_{\rm A} + r_{\rm X}}{\sqrt{2}(r_{\rm B} + r_{\rm X})},\tag{1}$$

conduction bands, or very shallow. 11-13 Therefore, there is a huge amount of interest in developing high-performance perovskitebased optoelectronic devices including, but not limited to, solar cells, light-emitting devices (LEDs), photo-/radiation-detectors, and scintillators. 14-17 Especially, the power conversion efficiency (PCE) of perovskite-based solar cells (PSCs) has swiftly climbed to a certified 23.7%, 18 since Miyasaka et al. reported the first PSC with a 3.8% PCE in 2009.<sup>5</sup> The halide perovskites that have been most widely studied in the literature exhibit a 3D crystal structure with a general chemical formula of ABX3, where A is a monovalent cation such as methylammonium (CH<sub>3</sub>NH<sub>3</sub><sup>+</sup>, MA<sup>+</sup>), formamidinium (HC(CH<sub>2</sub>)<sub>2</sub><sup>+</sup>, FA<sup>+</sup>), and Cs<sup>+</sup>, B is a divalent cation such as Pb<sup>2+</sup> and Sn<sup>2+</sup>, and X is a halide ion such as I<sup>-</sup>, Br<sup>-</sup>, and Cl<sup>-</sup>. Fig. 1a shows the crystal structure of 3D halide perovskites of ABX<sub>3</sub>. Empirically, the crystal structure of an ABX<sub>3</sub> compound is determined by Goldschmidt's tolerance factor t, defined as, <sup>19</sup>

<sup>&</sup>lt;sup>a</sup> School of Engineering, Brown University, Providence, RI 02912, USA. E-mail: yuanyuan\_zhou@brown.edu

b College of Environmental Science and Engineering, Shanghai Jiao Tong University, Shanghai 200240. P. R. China. E-mail: yixin.zhao@situ.edu.cn

<sup>&</sup>lt;sup>c</sup> Shanghai Institute of Pollution Control and Ecological Security, Shanghai 200092, P. R. China

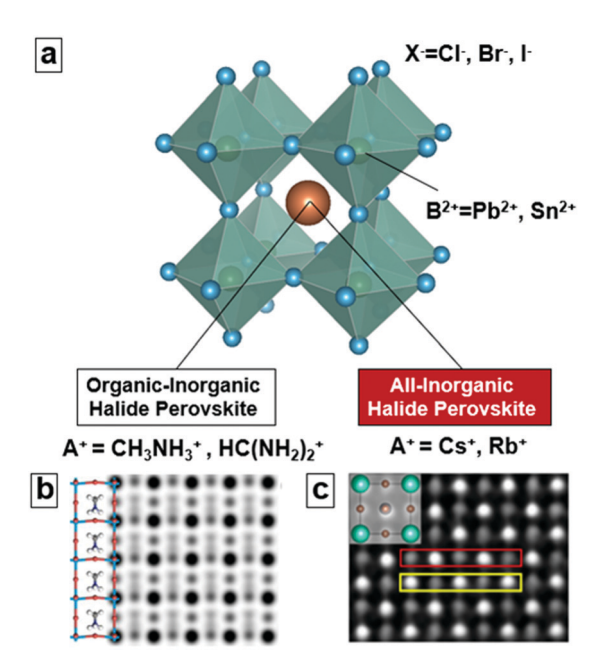


Fig. 1 (a) Schematic representation of the typical ABX<sub>3</sub> crystal structure of halide perovskites. The nature (organic or inorganic) of A-site ions determines the types of all-inorganic halide perovskites and hybrid organic-inorganic halide perovskites. (b) The structural model and simulated projected potential map of the prototypical MAPbl<sub>3</sub> HHP based on high-resolution TEM characterization. Adapted from ref. 31 with permission requested from the American Association for the Advancement of Science (AAAS). (c) The structural model and phase image of the prototypical CsPbBr<sub>3</sub> IHP based on based on high-resolution TEM characterization. Adapted from ref. 32 with permission requested from the American Chemical Society (ACS).

where  $r_A$ ,  $r_B$ , and  $r_X$  are the ionic radii of the A-cation, B-cation, and X-anion. When t is between 0.8 and 1.0, the crystal favors a 3D perovskite structure. When t > 1.0, a NH<sub>4</sub>CdI<sub>3</sub>-type crystal structure is usually favored. When t < 0.8, a CsNiBr<sub>3</sub>-type crystal structure is most likely to form. Besides t, the octahedral factor  $\mu$  is another important empirical parameter, which is defined as, <sup>20,21</sup>

$$\mu = r_{\rm B}/r_{\rm X},\tag{2}$$

where  $r_{\rm B}$  and  $r_{\rm X}$  are the radii of the B-cation and X-anion. A  $\mu$  value of 0.4 to 0.9 contributes to the formation of stable BX<sub>6</sub> octahedra.<sup>21</sup> Due to these structure restrictions (simultaneous satisfaction of both t and  $\mu$  conditions), there are actually a very limited number of combinations of A, B, and X ion types that can lead to 3D perovskites. The most popularly studied 3D halide perovskites amongst them are methylammonium lead halide (CH3NH3PbX3, MAPbX3), formamidinium lead halide (HC(NH<sub>2</sub>)<sub>2</sub>PbX<sub>3</sub>, FAPbX<sub>3</sub>), cesium lead iodide (CsPbX<sub>3</sub>), and cesium tin halide (CsSnX<sub>3</sub>). Nevertheless, recent research progress in the HP field has revealed a lot more perovskite-inspired compounds, which show very interesting optoelectronic and chemical properties. These new compounds typically include the layered Ruddlesden-Popper type perovskite phases (A2BX4),22,23 layered Dion-Jocobson type perovskite phases (ABX<sub>4</sub>), <sup>24,25</sup> A<sub>3</sub>B<sub>2</sub>X<sub>9</sub> compounds, <sup>26,27</sup> A<sub>2</sub>B'B"X<sub>6</sub> or A<sub>2</sub>BX<sub>6</sub> double-perovskite phases, <sup>28</sup>

and A<sub>4</sub>BX<sub>6</sub> compounds, <sup>29,30</sup> all of which have been later embraced in the broad HP family.

Halide perovskites can be broadly divided into two types, hybrid organic-inorganic halide perovskites (HHPs) and inorganic halide perovskites (IHPs), depending on the chemical nature (organic or inorganic) of A-site ions, as shown in Fig. 1. Fig. 1b and c shows the high-resolution transmission electron microscopy (TEM) characterization results of the prototypical MAPbBr<sub>3</sub> HHP and CsPbBr<sub>3</sub> IHP, where the structural difference in the A-site ion of ABX<sub>3</sub> could be resolved at the atomic scale. The CsPbBr<sub>3</sub> IHP contains only symmetric, spherical cations in A-sites, while organic, asymmetric, and polar MA<sup>+</sup> cations can be observed in the MAPbI<sub>3</sub> HHP in Fig. 1b. The polar MA<sup>+</sup> cations could also have varied orientations at specific atomistic sites in the MAPbI<sub>3</sub> HHP. Until now, regarding the photovoltaic (PV) applications, the state-of-the-art PSCs have still employed HHPs as light absorbers. 33-35 However, it is generally argued that these HHP-based PSCs suffer from low intrinsic or thermodynamic stability issues due to the inclusion of organic MA<sup>+</sup> and FA<sup>+</sup> cations, which are volatile in nature. This significant issue has stimulated a surge of interest in using IHPs to replace HHPs for some PV applications.36-38 Moreover, for non-PV optoelectronic applications such as LEDs, radiation-detectors, and scintillators, IHPs have shown even more promise due to their suitable optical properties, as well as much more robust stability under external stimuli such as electric bias and radiation.<sup>39</sup> Although a lot of attention has been attracted by IHPs for the sake of the superior stability over their HHP counterparts, the chemical stability of IHPs themselves has also become a concern. In this review, first, insights into the origins of IHP stability and instability are provided. Then, the reported strategies in the literature that address the instability issues of IHPs are reviewed. Finally, we present perspectives on promising future directions towards stable IHP materials and devices.

# Mechanistic origins of stability and instability of inorganic halide perovskites

The low stability of typical HHPs like MAPbI<sub>3</sub> has been noticed since the early stage of PSC research. 41 Nagabhushana et al. 40,42 experimentally measured the formation enthalpies of the MAPbI<sub>3</sub> HHP based on acid-solution calorimetry, showing that MAPbI<sub>3</sub> is intrinsically/thermodynamically unstable and prone to decomposition to its binary halide components (MAI and PbI<sub>2</sub>) even in the absence of external stimuli such as moisture, oxygen, heat, and irradiation. This is highly consistent with the theoretical prediction by Zhang et al.40,43 who show the decomposition reaction of MAPbI3,

$$MAPbI_3 \rightarrow MAI + PbI_2 \tag{3}$$

is exothermic (at 0 K and zero pressure), independent of atmospheric factors (see Fig. 2a). Substitution of A-, B-, and X-site ions with other corresponding ions can tune the formation energies, resulting in more stable compounds. In

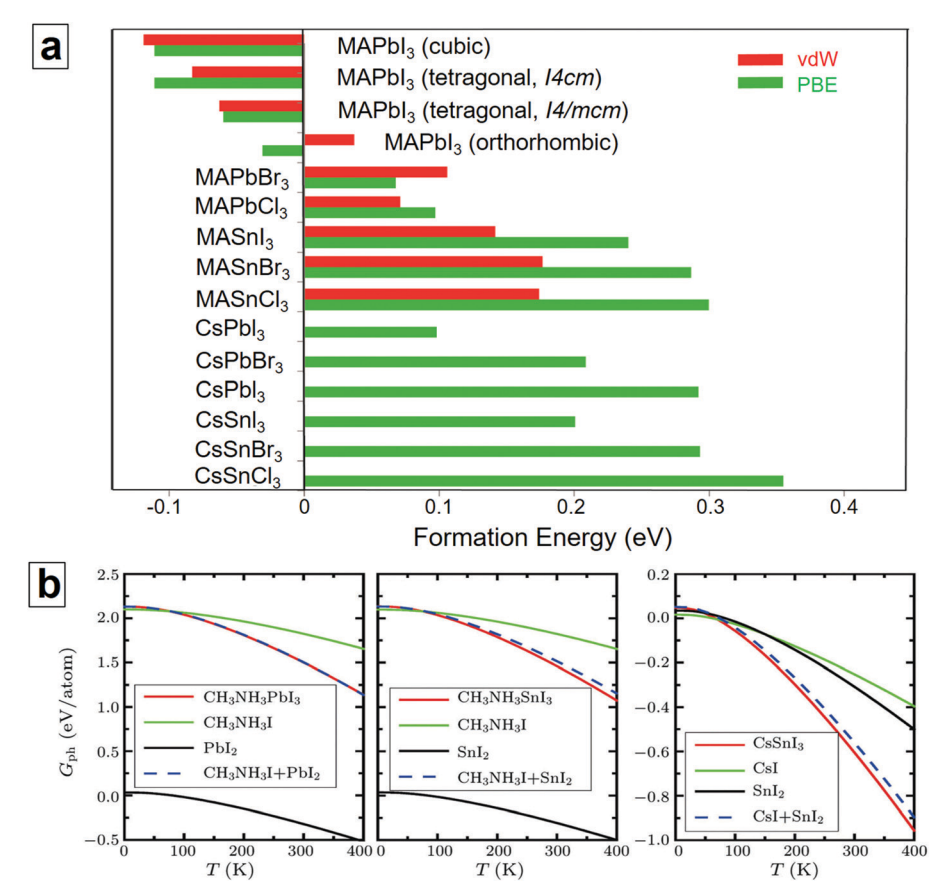


Fig. 2 (a) Calculated formation energies for different HHPs or IHPs with Perdew-Burke-Ernzerhof (PBE) and van der Waals (vdW) exchange-correlation functionals. A positive number indicates that the compound is stable at 0 K. (b) Calculated vibrational free energy of the MAPbl<sub>3</sub> HHP, MASnl<sub>3</sub> HHP and CsSnl<sub>3</sub> IHP as a function of temperature (7). Adapted from ref. 40 with permission requested from Chinese Physical Society,

particular, for these IHPs with A-sites occupied by Cs<sup>+</sup>, the formation energies become generally higher than those of the HHP counterparts. This is consistent with the experimental observations. 40,43-45 Zhang et al. 40,43 have further determined the true thermodynamic stability using the Gibbs free energy as shown in Fig. 2b, which takes into account the contributions from internal energy, pressure, and temperature (vibrational and configurational entropy). It is shown that the vibrational contribution is comparable for the reactant and products of reaction (3) and therefore does not influence the MAPbI3 or MASnI3 stability. However, for the configurational entropy, the energy differences for MAI with different MA<sup>+</sup> orientations are much smaller than those for MAPbI<sub>3</sub> and MASnI<sub>3</sub> HHPs. 40,43 This suggests that MAI may have higher configurational entropy than MAPbI<sub>3</sub> and MASnI<sub>3</sub> HHPs, decreasing the stability of the perovskite structure. 40,43 Once MA<sup>+</sup> ions are fully replaced by Cs<sup>+</sup>, the vibrational entropy can slightly enhance the stability of the perovskite structure, as the vibrational free energy decreases faster than those decomposition products as a function of temperature as shown in Fig. 2b. 40,43 Meanwhile, the configuration entropy becomes less important in the all-inorganic compounds as the Cs<sup>+</sup> cation itself is symmetric without multiple configurations. 40,43 All these combined experimental-theoretical results basically explain the superior intrinsic or thermodynamic stability of IHPs over HHPs.

There are some other factors contributing to the possibly enhanced stability of IHPs over HHPs. Aristidou et al. 47,48 have shown that MAPbI<sub>3</sub> HHP degradation under light and oxygen is initiated by the reaction of superoxide (O<sup>2-</sup>) with the protonated MA<sup>+</sup> moiety in HHPs. In this context, inorganic cations such as Cs<sup>+</sup> are free of acid protons, which improves the tolerance of perovskites to oxygen under light. Also, many theoretical and experimental studies have shown that IHPs are purely halideion conductors while both organic-cations and halide-ions are mobile in HHPs, 49-52 implying IHPs have an inherently more rigid crystal structure to resist electrochemical changes under external stimuli.

While the above analyses provide reasonable rationales for considering IHPs as more stable materials than the HHP counterparts, in fact, many important IHPs are found to be not stable enough under external stimuli such as moisture, light, heat, and oxygen. In a recent perspective article by Ju et al.,46 the degradation mechanisms for all kinds of halide perovskites have been well summarized (Fig. 3), which include polymorphic transition, hydration, decomposition, and oxidation. Different from HHPs, IHPs are free of hygroscopic organic cations, in which context the hydration of IHPs may not occur frequently. Thus, the dominating degradation mechanism for IHPs can be either polymorphic transition, decomposition, oxidation, or

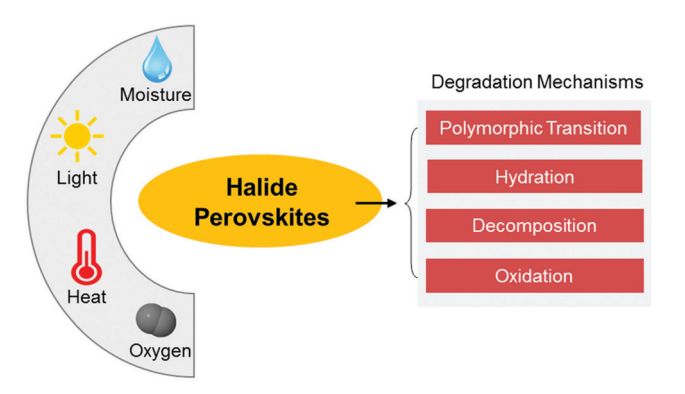


Fig. 3 Illustration of degradation mechanisms of halide perovskites under key environmental factors (moisture, light, heat, and oxygen). Adapted from ref. 46 with permission requested from Elsevier

their combinations. It will also be highly dependent on the specific perovskite composition.

The most typical lead-based IHP composition is CsPbI<sub>3</sub>. The CsPbI<sub>3</sub> perovskite is usually known as the 'black' polymorph (α-phase), and it exhibits a bandgap of 1.8 eV, which is suitable for PV applications. However, the tolerance factor (t) of CsPbI<sub>3</sub> is calculated as 0.80 based on the ionic radii of Cs<sup>+</sup>, Pb<sup>2+</sup>, and I<sup>-</sup> (Table 1). The relatively low t results in the structural instability of  $\alpha$ -CsPbI<sub>3</sub> (space group  $Pm\bar{3}m$ ; a = 6.201 Å), which can easily transform to its 'yellow' nonperovskite polymorph (δ-phase, space group Pnma) that is thermodynamically more stable at ambient temperature. This perovskite-to-nonperovskite polymorphic transition becomes even more facile when moisture is present, although the catalytical role of moisture has not been fully understood. For lead-free IHPs, the most typical compound is CsSnI<sub>3</sub>. While the CsSnI<sub>3</sub> IHP (γ-phase at room temperature) has an ideal bandgap of 1.3 eV for single-junction PSCs, this compound is unstable mainly due to the facile

Table 1 Estimated radii of typical organic and inorganic ions in halide perovskites, which can be used for calculating the Goldschmidt's tolerance factor. The data are adopted from ref. 73-76

Ion type	Radius (Å)
Cs <sup>+</sup>	1.67
Rb <sup>+</sup>	1.52
$\mathrm{NH_4}^+$	1.46
$MA^{+}$	2.17
$FA^+$	2.53
$DMA^{+}$	2.72
$Pb^{2+}$	1.19
Sn <sup>2+</sup>	1.18
Ge <sup>2+</sup>	0.73
$Sn^{4+}$ $Ag^{+}$ $In^{3+}$ $Eu^{3+}$	0.69
$Ag^{+}$	1.15
In <sup>3+</sup>	0.80
Eu <sup>3+</sup>	0.95
Sb <sup>3+</sup>	0.76
Bi <sup>3+</sup>	1.03
$\mathrm{Ti}^{4+}$	0.61
$Mn^{2+}$	0.70
$I^-$	2.20
Br <sup>-</sup>	1.96
Cl <sup>-</sup>	1 9/1

oxidation of Sn2+ to Sn4+ in ambient air.6 In this context, the following sections will primary focus on discussing the stabilization protocols for these two materials (lead-based CsPbI<sub>3</sub> and lead-free CsSnI<sub>3</sub>) by addressing the polymorphic transition and oxidation issues, respectively. There are also some emerging IHP materials with relatively complex compositions (e.g. Cs<sub>2</sub>AgBiI<sub>6</sub>) which are thermodynamically prone to decompose regardless of the all-inorganic compositions, which will also be involved in the discussion. In order to present a clear overview of the current progress in stabilizing IHPs, the stability results of representative studies by various groups are summarized in Table 2. Nevertheless, these stability results may not be directly compared with each other since there are no standardized test conditions for evaluating perovskite materials and devices.

# Stabilization of lead-based inorganic halide perovskites

#### 3.1. Element doping/alloying - tuning the tolerance factor and inducing lattice strain

As described above, the low chemical stability of CsPbI3 is mostly due to the relatively low t (0.80) of this compound, <sup>44</sup> compared to that ( $\sim 0.91$ ) of its HHP counterpart MAPbI<sub>3</sub>. The low t is attributed to the small ionic size of the Cs cation. Obviously, t can be tuned by incorporation of new ions in the ABX3 crystal structure, which will lead to a change in the average radii of A-, B-, or X-site ions. Meanwhile, the size difference of the incorporated ions to A-, B-, or X-sites should be small enough to avoid phase segregation. For the A-site, organic cations such as FA<sup>+</sup> and MA<sup>+</sup> are good candidates for tuning t and stabilizing the perovskite phase. But the resulting stabilized perovskite contains the volatile FA<sup>+</sup> and MA<sup>+</sup> cations regardless of their small amount, making intrinsic thermal stability a concern. Unfortunately, there is no inorganic cation suitable for increasing t in the CsPbI<sub>3</sub>-based compound as Cs is the largest-size Group-I element that is nonradioactive. Another way to increase t is to substitute some portion of I anions with the smaller-size Br, which will form CsPbI<sub>3-r</sub>Br<sub>r</sub> alloy perovskites and retain the all-inorganic composition. Sutton et al. have reported the enhanced phase stability of CsPbI<sub>3-x</sub>Br<sub>x</sub> compared with CsPbI<sub>3</sub> for the first time, 54,55 which is further confirmed by several following reports.<sup>56-61</sup> However, the Br alloying induces an undesired blue shift of the absorption edge and an enlarged bandgap, e.g. the popularly studied CsPbI2Br exhibits an absorption edge of 680 nm and a bandgap of 1.9 eV.<sup>62</sup> Note that the bandgap of CsPbI<sub>3</sub> is  $\sim$ 1.8 eV, which is already too large as absorber materials in single-junction solar cells. In this context, there is a need to develop strategies that enhance the perovskite phase stability without increasing the bandgap, and doping/alloying the B-site of CsPbI3 with various smaller-size metal cations such as Sn<sup>2+,63-65</sup> Ge<sup>2+,66</sup>,  $Bi^{3+},^{67}Sb^{3+},^{68}Eu^{3+},^{53,69}$  and  $Mn^{2+70,71}$  is employed to achieve this goal (Fig. 4a).72

Sn<sup>2+</sup> exhibits the most similar chemical properties to Pb<sup>2+</sup> and the radius of Sn<sup>2+</sup> is only slightly smaller than Pb and thus

The stability results from representative studies on IHPs

Perovskite composition	Stabilization method	Material stability	Device stability	Ref.
$CsPbI_3$	Nanocrystals	No obvious degradation for 60 days (humidity: n/a; temperature:	Best PCE: 10.77%; PCE increases after 64 days storage (humidity: n/	37
$\mathrm{CsPbI}_3$	Crystal dimensionality ('quasi-2D')	No obvious degradation for 7 days (humidity: n/a, temperature: 100 °C, light: n/a; atmosphere: dry air)	a, temperature: M1, 11g/m: 11/4, attnospirere: my an, unchrappenateur. Best PCE: 11.8%; PCE retains ~ 90% of the initial performance after 30 days storage (humidity: n/a, temperature: 100 °C, light: n/a; ormognese, cir., unga concentrate).	96
$\mathrm{CsPbI}_3$	PVP additive	No obvious degradation for 80 days (humidity: n/a; temperature: n/a; light: n/a; atmosphere: ambient air)	authospitete: an, unencapoutated)  Best PCE: 10.74%; PCE retaining $\sim$ 80% of the initial performance after 21 days storage (humidity: 45–55% RH; temperature: 50 °C; light: $n/\alpha$ : atmosphere: air: unencapoulated)	84
$\mathrm{CsPbI}_3$	Zwitterion additive	No obvious degradation for 60 days (humidity: n/a; temperature: n/a; light: n/a; atmosphere: ambient air)	Best PCE: 11.4%; PCE retaining ~85% of the initial performance after 30 days storage (humidity n/a; temperature: n/a; light: n/a; atmosthere: ambient air: inencansulated)	105
$CsPbI_3$	Ctystal dimensionality ('quasi-2D')	No obvious degradation for 40 days (humidity; 20% RH; temperature: 20 °C; light: n/a; atmosphere: air)	Best PCE: 12.4% PCE retaining 93% of the initial performance after 40 days storage (humidity: 20% RH; temperature: 20 °C; light: n/a; atmosphere: air; unencapsulated	97
$\mathrm{CsPbI}_3$	Processing & microstructure engineering	No obvious degradation for 60 days (humidity: n/a; temperature 300 $^{\circ}C$ light: n/a; atmosphere: dry N <sub>2</sub> )	Best PCE: 15.7% (certified) PCE retaining > 95% of the initial performance after 500 h continuous operation" (humidity: n/a; temperature: 25 °C; light: one-sun: atmosshere: drv N.s. encansulated)	106
$\mathrm{CsPbI}_2\mathrm{Br}$	Eu-element doping	No obvious degradation for 50 h (humidity: 20–40% RH; temperature: n/a; light: n/a; atmosphere: dry air)	Best PCE: 13.71% PCE retaining 68% of the initial performance after 370 h continuous operation <sup>a</sup> (humidity: n/a; temperature: n/a; light: one-sun; atmo-cabara: dr. N. 1.1.00000001114cd.)	53
$\mathrm{CsPbI}_3$	Bi-element doping	No obvious degradation for 7 days (humidity: n/a; temperature: n/a; light: n/a; atmosphere: dry air)	spirer, up 12, unitrapsulated) Best PCE: 13.21%  PCE retaining 68% of the initial performance after 7 days storage (humidity, 0, teamperature, n) a strong short properties of the content	29
$\mathrm{CsSnI}_3$	Grain encapsulation (SnCl <sub>2</sub> additive)	No obvious degradation for 3 h (humidity: 25% RH; temperature: RT; light: n/a; atmosphere: air)	Rest PCE: 3.56% PCE retention of 80% for 5 h storage (humidity: 25% RH; temperature 50.%; stronghere: air: unancapulated)	107
$\mathrm{CsSn}_{0.5}\mathrm{Ge}_{0.5}\mathrm{I}_3$	Native-oxide passivation	No obvious degradation for 72 h (humidity: 80% RH; temperature: 45 $^{\circ}\text{C}$ ; light: one-sun; atmosphere: air)	Best PCE: 7.11% PCE retention of 90% after 500 h continuous operation <sup>a</sup> (humidity: 0; temperature: 45 °C; atmosphere: dry N <sub>2</sub> ; light: one-sun; unencapsulated)	108

Note: the environmental conditions are adopted from the original references, some of which may have not mentioned the exact humidity, temperature, light, and atmosphere conditions (marked as n/a). The operational stability of the device.

Table 2

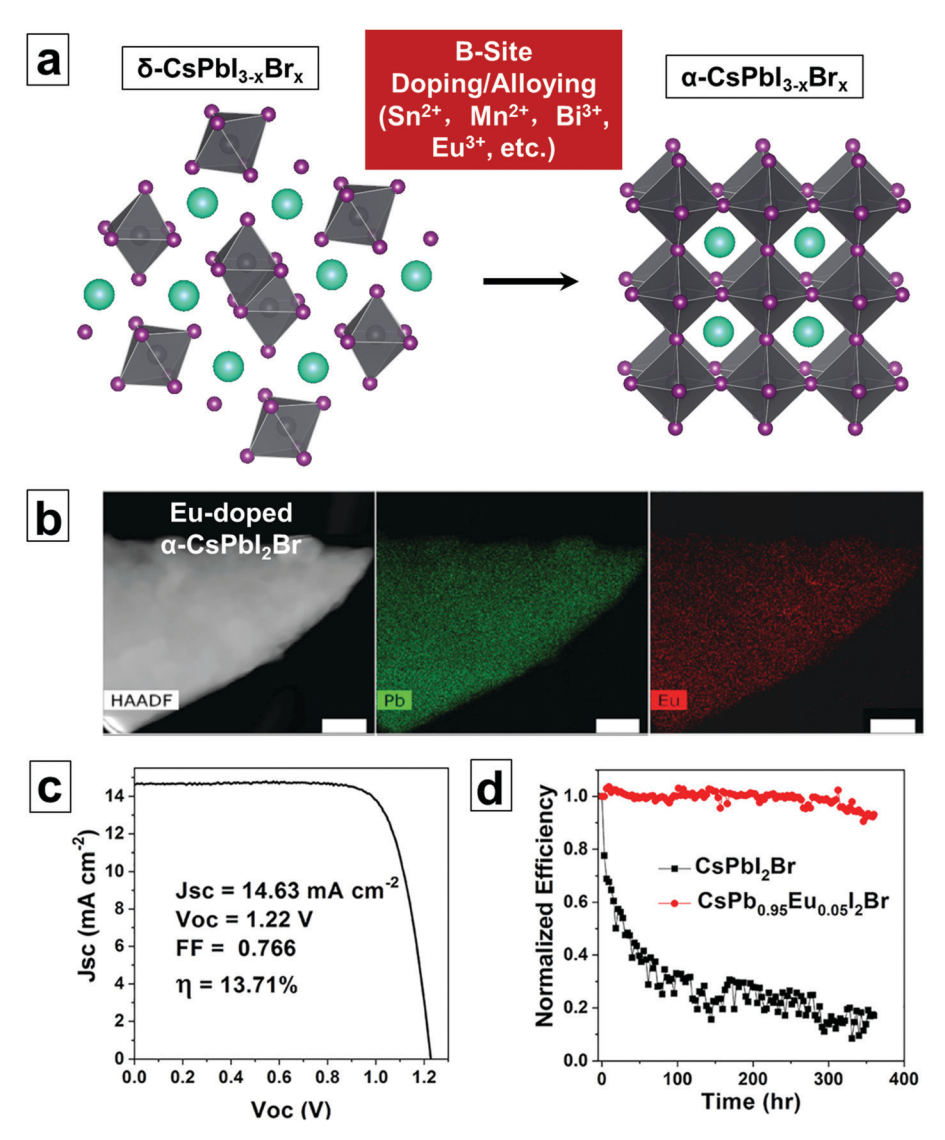


Fig. 4 (a) Schematic illustration of stabilization of CsPbI<sub>3-x</sub>Br<sub>x</sub> using a B-site doping/alloying strategy. (b) High-angle annular dark-field imaging (HAADF) TEM image of Eu-doped CsPbl<sub>2</sub>Br and the corresponding Pb and Eu elemental mapping. (c) Current density-voltage curve of the best-performing Eu-doped CsPbl<sub>2</sub>Br PSCs. (d) Comparison of the stability of CsPbl<sub>2</sub>Br PSCs with and without Eu doping. Adapted from ref. 53 with permission requested from Elsevier.

CsPb<sub>1-r</sub>Sn<sub>r</sub>I<sub>3</sub> can easily form, which enables effective tuning of the tolerance factor. It is shown that although CsSnI3 is unstable in ambient air due to the oxidation sensitivity of Sn<sup>2+</sup>, CsPb<sub>1-x</sub>Sn<sub>x</sub>I<sub>3</sub> (in the material form of nanocrystals) with a low Sn2+ content can exhibit high phase-stability in ambient conditions as well as extended absorption in the near-infrared-red region.<sup>64</sup> Sn<sup>2+</sup> substitution in CsPbI<sub>3</sub> could be used in combination with Br substitution, resulting in stable CsPb<sub>1-x</sub>SnI<sub>3-x</sub>Br<sub>x</sub> alloy perovskite phases with suitable bandgaps. 63 Mn2+ incorporation has been shown to be highly effective in stabilizing either CsPbI<sub>3</sub> perovskite thin films or nanocrystals.<sup>70</sup> Since the size difference between Mn<sup>2+</sup> and Pb<sup>2+</sup> is relatively large, only a very slight amount of Mn2+ can be possibly accommodated in the CsPbI<sub>3</sub> crystal structure with the occurrence of phase separation. Theoretical calculations have revealed that the Mn<sup>2+</sup> doping levels are located within the conduction band. Therefore, Mn-doping induces negligible change in the absorption features. In addition, Mn<sup>2+</sup> doping has shown a positive effect on thin film formation.<sup>71</sup> These combinations lead to the enhancement of the photovoltaic (PV) performance of CsPbI<sub>3</sub> or CsPbI<sub>3-r</sub>Br<sub>3</sub> PSCs.<sup>71,77</sup> Aliovalent B-site doping with Bi<sup>3+</sup>, Sb<sup>3+</sup>, or Eu<sup>3+</sup> is also proven to strongly enhance the phase stability of the CsPbI<sub>3</sub> or  $CsPbI_{3-x}Br_x$  perovskites. In addition to tuning the tolerance factor, such aliovalent doping induces slight distortion of the perovskite crystal structure via the naturally coupled formation of iodine vacancies. These additional vacancies could induce lattice strain in the crystal, showing a positive effect in stabilizing the perovskite crystal structure. Energy dispersive spectroscopy studies show a uniform dopant element distribution when lessthan-5 mol% Bi<sup>3+</sup> or Eu<sup>3+</sup> is incorporated (Fig. 4b).<sup>53,67,69</sup> In a recent study,53 the Eu-doped CsPbI2Br PSC with a wide bandgap of 1.9 eV show an impressive PCE of 13.71% (Fig. 4c). As seen

in Fig. 4d, the high performance could be retained with 93% of the initial efficiency after 350 h operation of the PSC under 100 mW cm<sup>-2</sup> continuous white-light illumination using the maximum-power point-tracking measurement, demonstrating much better stability over the doping-free CsPbI<sub>2</sub>Br PSC. All these studies clearly demonstrate the effectiveness of various doping methods in stabilizing IHPs, and one promising future direction will be to explore co-doping strategies with multiple elements, which may have synergic and optimal effects in stabilizing IHP materials and devices.

#### 3.2. Nanocrystal-induced phase stabilization

While early studies have revealed that CsPbI<sub>3</sub> perovskite bulk thin films or large crystals are not stable in the α-phase at ambient temperature, 78 the CsPbI<sub>3</sub> nanocrystals that are synthesized via solution-phase methods have exhibited an interesting phenomenon of size-dependent phase-stability. Kovalenko and coworkers have found that the α-CsPbI<sub>3</sub> nanocrystals with 100 to 200 nm size quickly degrade into the δ-phase, but the α-CsPbI<sub>3</sub> nanocrystals with 4 to 15 nm size can stay in the α-phase upon storage for one month at ambient temperature.<sup>79</sup> The nanocrystal-induced stabilization of the CsPbI3 perovskite could be reasonably attributed to the high surface energy of nanocrystals or the high surface micro-strain on nanocrystals. Later, Swarnkar et al. have for the first time demonstrated the use of CsPbI<sub>3</sub> perovskite nanocrystals in PSCs as shown Fig. 5a, and reported a high PCE of 10.77% (a record at the time) with a very high open-circuit voltage of 1.23 V.37 A typical TEM image of the as-studied CsPbI3 perovskite nanocrystals is exhibited in Fig. 5b, showing the perfect perovskite lattice, and these

nanocrystals retain their α-phases after 60 days storage in ambient conditions, as indicated from the XRD results in Fig. 5c. Regarding CsPbI<sub>3</sub> perovskite nanocrystal based PSCs, the surface ligands of the nanocrystals play a double-edgedsword effect. On one hand, the ligands serve as a capping layer that protect the nanocrystals from segregation and then coarsening into large-size nanocrystals or bulk crystals that are intrinsically unstable. On the other hand, the ligands may block the conduction of charge carriers to some extent. To address this dilemma, in a later study by Luther et al., a posttreatment using organic halide salts (e.g. FAX) was employed to enhance the electronic coupling between CsPbI3 perovskite nanocrystals while maintaining the nanocrystal morphology.<sup>36</sup> The mobility of CsPbI<sub>3</sub> perovskite nanocrystal assembled thin films was increased from 0.23 to 0.50 cm<sup>2</sup> V<sup>-1</sup> s<sup>-1</sup> with retained high chemical stability. The resulting CsPbI3 nanocrystal based PSCs exhibited a certified PCE of 13.43%. While there are a few other excellent studies on developing CsPbI3 perovskite nanocrystal based PSCs, 36,80-82 existing effort in this direction is still highly limited in the literature. Future effort in tailoring surface defects, ligand-crystal interaction, and the morphology of nanocrystals, as well as understanding and engineering of device structures, will lead to more stable and efficient IHP nanocrystal based solar cells.

#### 3.3. Additive-crystal interaction

Incorporation of suitable nonvolatile additives in CsPbI<sub>3</sub> precursor solutions is an alternative method to crystallize and stabilize CsPbI<sub>3</sub> in its perovskite phases, because these additives are able to tailor the surface energy, reduce the grain size, and form

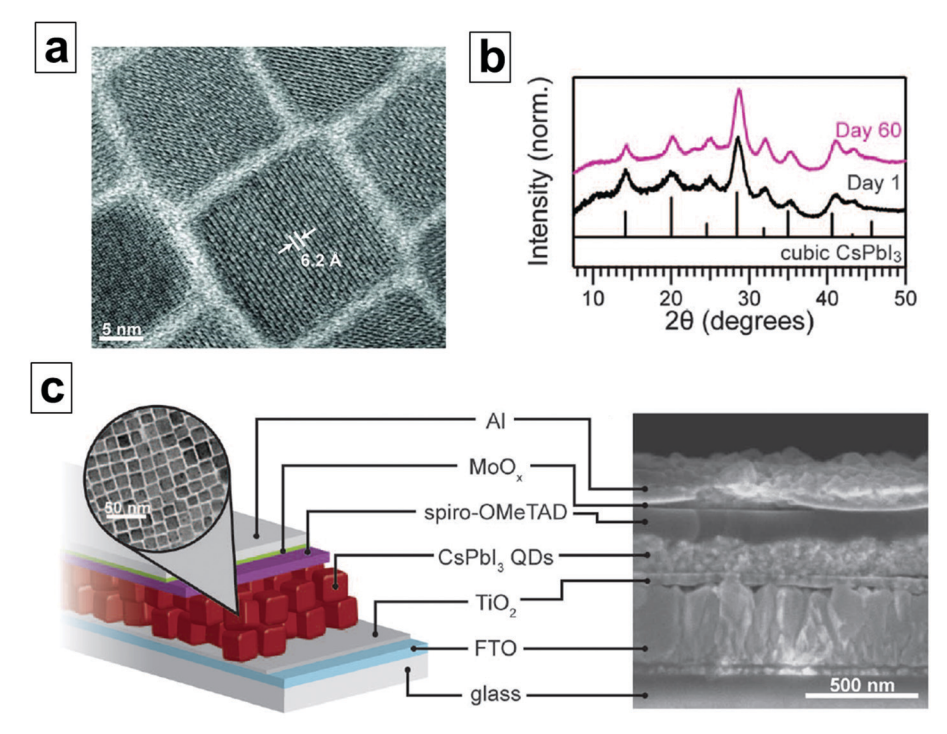


Fig. 5 (a) Schematic illustration of the CsPbI $_3$  nanocrystal based perovskite solar cells. (b) TEM image of colloidal  $\alpha$ -CsPbI $_3$  nanocrystals. (c) XRD patterns of the α-CsPbl<sub>3</sub> nanocrystals after storage in ambient conditions for 1 and 40 days. Adapted from ref. 37 with permission requested from AAAS.

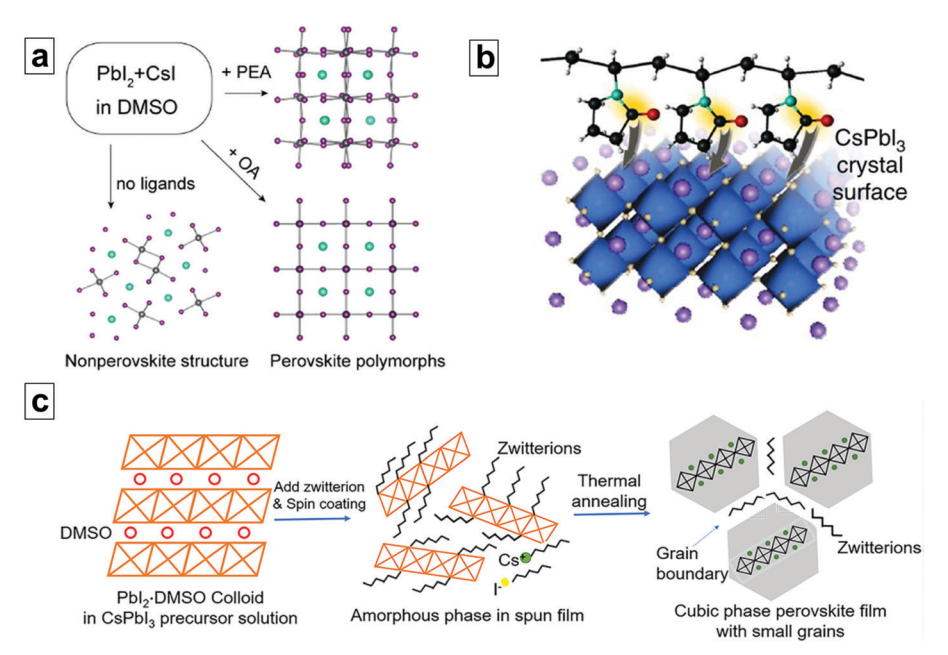


Fig. 6 (a) Schematic illustration showing the formation of  $\alpha$ - and  $\beta$ -CsPbl $_3$  using OA and the PEA ligand additive. Adapted from ref. 83 with permission requested from ACS. (b) Schematic illustration of stabilizing the CsPbI<sub>3</sub> perovskite using PVP. Adapted from ref. 84 with permission under the Creative Commons Attribution 4.0 International License. (c) Schematic illustration of stabilizing the CsPbl3 perovskite phase with zwitterions. The zwitterion molecules segregate at grain boundaries during the CsPbl<sub>3</sub> perovskite crystallization. Adapted from ref. 85 with permission requested from Elsevier.

nanoscale encapsulation layers of CsPbI<sub>3</sub> perovskite grains. The first type of additives is long-chain ammonium cations. As shown in Fig. 6a, Fu et al. 83 have shown that the incorporation of oleylammonium (OA+, ~1.7 nm in length) in the solution processing stabilizes the CsPbI<sub>3</sub> perovskite in the cubic α-phase whereas the use of phenylethylammonium (PEA $^+$ ,  $\sim 0.6$  nm in length) additives stabilizes the CsPbI<sub>3</sub> perovskite in the tetragonal β-phase where the octahedra are slightly tilted. Note that the exact crystal structure of the β-CsPbI<sub>3</sub> perovskite is not fully revealed yet in that study. A plausible mechanism responsible for this method is the strong molecular interaction of the additive phases with as-crystallized CsPbI3, which tunes the surface energy and stabilizes the CsPbI3 perovskite phase kinetically. With either OA<sup>+</sup> and PEA<sup>+</sup> additives, the CsPbI<sub>3</sub> perovskites show no obvious phase degradation after 4 month storage in ambient conditions.83

Polymers are another type of effective additives. Li et al. 84 have incorporated poly-vinylpyrrolidone (PVP) into the solutionprocessing of CsPbI3 perovskites. They have claimed that PVP has amide groups with chemical properties similar to -NH3 groups in those ammonium-based additives.<sup>84</sup> Therefore, PVP also interacts with CsPbI3 via molecular bonding (Fig. 6b). The as-deposited CsPbI3 perovskite thin films with PVP additives are highly stabilized, exhibiting impressively long carrier diffusion lengths of  $\sim 1.5 \, \mu m$ . The resulting PSCs show a PCE of 10.74%, close to that for the CsPbI<sub>3</sub> perovskite nanocrystal based PSCs. Regarding the device stability, 75% of the initial PCE is retained after the encapsulated PSC is exposed to ambient air with  $\sim$  50% relative humidity (RH) for 500 h. In another study by Beomjin et al.,86 the poly(ethylene-oxide) (PEO) polymer has also been used to inhibit the  $\delta$ -phase formation during the solution processing of CsPbI<sub>3</sub> perovskite thin films and promote low-temperature perovskite crystallization. High-performance red-light LEDs (brightness of  $\sim 101$  cd m<sup>-2</sup>; external quantum efficiency of 1.12%; emission bandwidth of 32 nm) are achieved. Although PEO doesn't have the necessary functional groups to form strong chemical bonds with CsPbI3 like PVP, Beomjin et al.84 have found that PEO scaffolds provide a confined environment for the crystallization of the CsPbI3 perovskite, leading to the formation of CsPbI3 perovskite small-grains that are fully encapsulated. Note that, similar to the case of CsPbI<sub>3</sub> perovskite nanocrystals, the phase stability increases with a decrease in the grain size in the CsPbI3 perovskite bulk thin film. This is partially responsible for the good stability of PEO-incorporated CsPbI<sub>3</sub> perovskite thin films. Since polymers are a very large family of materials with highly tunable molecular structures and properties, it may be possible to develop more effective additives for stabilizing IHPs using synthetic polymers with specially-designed functional groups.

Large polar organic molecule additives are also useful for making stable CsPbI3 perovskite thin films. Recently, Wang et al. have shown that sulfobetaine zwitterion additives exhibit an obvious effect in stabilizing CsPbI3 perovskites and achieved a PCE of 11.4% in the resulting PSCs. 85 The proposed mechanism for zwitterion-induced CsPbI3 perovskite stabilization is schematically shown in Fig. 6c. It is claimed that the zwitterion not only hinders the rapid crystallization of the CsPbI<sub>3</sub> perovskite in the conventional additive-free 'one-step' deposition process, but also induces a decrease in the grain size in the resulting thin film.<sup>85</sup> The grain size in this perovskite thin film is only  $\sim 30$  nm, similar to that of the CsPbI<sub>3</sub> perovskite nanocrystals. The grain size decrease could be attributed to the enhanced heterogeneous

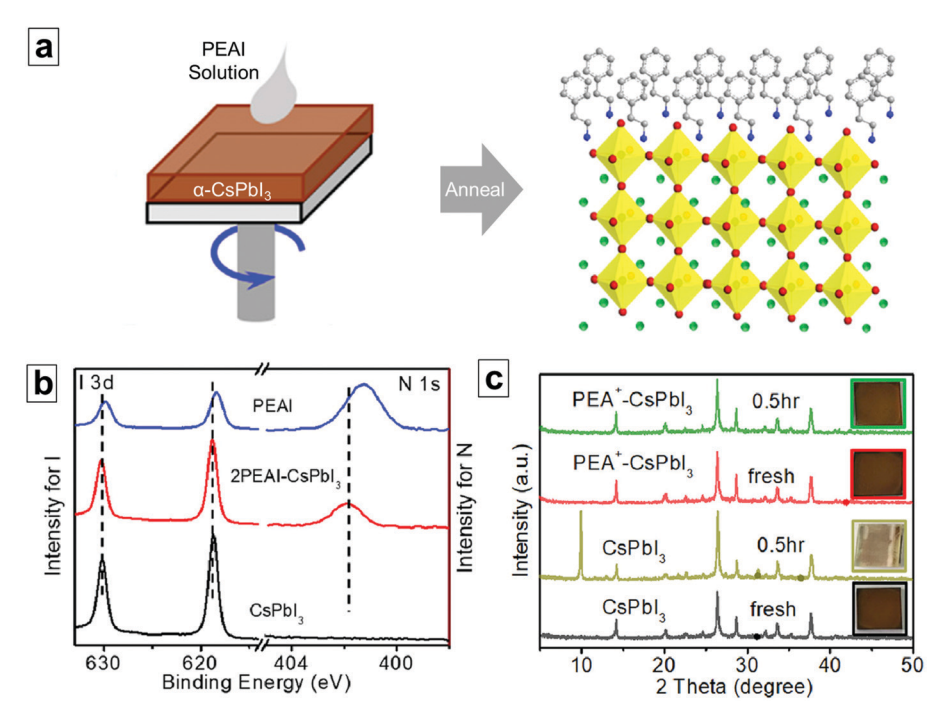


Fig. 7 (a) Schematic illustration of the CsPbI<sub>3</sub> perovskite thin film surface terminated with PEAI. (b) XPS spectra of the PEA-CsPbI<sub>3</sub> perovskite compared with CsPbI<sub>3</sub> and PEAI thin films. (c) Stability of the CsPbI<sub>3</sub> and PEAI-treated CsPbI<sub>3</sub> thin films upon exposure to ambient conditions (~85% RH, RT) for 0.5 h. Adapted from ref. 91 with permission requested from Elsevier.

nucleation sites and the constraint effects induced by the largemolecule polar zwitterion.<sup>85</sup>

The use of other types of additives such as HI has been also demonstrated for CsPbI<sub>3</sub> perovskite stabilization, although the underlying mechanisms may still be under debate. For example, Heo et al. and Xiang et al. 87,88 have both observed that HI significantly reduces the processing temperature, resulting in stable α-CsPbI<sub>3</sub> perovskite thin films. Tensile lattice strain is observed in such α-CsPbI<sub>3</sub> perovskite thin films by Xiang et al.,87 which may contribute to the phase stability. However, it has been recently argued by Ke et al. 76 and Noel et al. 89 that the HI additive decomposes DMF, in situ forming dimethylammonium (DMA<sup>+</sup>). Ke et al. 76 have claimed that DMA<sup>+</sup> with an ionic radius of 0.272 nm could be incorporated in the perovskite structure, forming  $Cs_{1-x}DMA_xPbI_3$  (x = 0.2 to 0.5) with more ideal tolerance factors.<sup>76</sup> In order to elucidate this discrepancy regarding the role of the HI additive, more systematic studies may be valuable in the future. Nevertheless, this HI-additive method has been combined with the PEA+ additive method by Wang et al., 90 leading to CsPbI3-based PSCs with PCEs up to 15.07%. It is promising that this PSC keeps 92% of its initial PCE after two months storage in ambient conditions (20 to 30% RH at  $\sim 25$  °C). 90

#### 3.4. Surface post-treatment or functionalization

Surface post-treatment of as-deposited thin films, leading to the formation of thin functionalization layers, is another new promising stabilization method for CsPbI3 perovskites. In a recent study by Wang et al.,91 a PEAI layer was solution-deposited on the top of a CsPbI<sub>3</sub> perovskite thin film, followed by thermal annealing (see Fig. 7a). This treatment doesn't produce layered perovskite phases on the film surface, because there is a relatively high energy barrier for the cation-exchange reaction of CsPbI<sub>3</sub> to PEA<sub>2</sub>PbI<sub>4</sub>. But instead, a PEA<sup>+</sup> cation-terminated surface is formed as shown in Fig. 7a. This is actually consistent with the previous report claiming that alkyl-ammonium cations stabilize CsPbI3 nanocrystals through replacement of the surface Cs<sup>+</sup> cations. 92 Wang et al. 91 have further shown this simple PEAI post-treatment not only significantly enhances the phase-stability of the thin film, but also forms a hydrophobic barrier for resisting moisture ingression. The resulting CsPbI<sub>3</sub> PSCs show an impressively high PCE of 13.5%. In a later approach by Wang et al.,93 PEABr has been used instead of PEAI, which simultaneously functionalizes the film surface and induces gradient Br-doping into the film bulk. The stabilized PCE output of CsPbI3-based PSCs is further improved to 16.3% and 91% of the initial PCE can be retained when the device is stored in N2 with 500 h continuous white-light LED illumination. 93 Beyond PEA+ cations, other organic cations with tailored functional groups such as NH3+C2H4NH2+C2H4NH3+94 may exhibit more beneficial effects on enhancing the stability of lead-based IHPs, which is an interesting research direction in the future.

#### Engineering of crystal symmetry and dimensionality

The cubic  $\alpha$ -CsPbI<sub>3</sub> polymorph (space group  $Pm\bar{3}m$ ) is the most commonly claimed in the reported CsPbI<sub>3</sub> perovskite thin films or nanocrystals. In fact, CsPbI3 also has two other perovskite polymorphs, tetragonal β-CsPbI<sub>3</sub> and orthorhombic  $\gamma$ -CsPbI<sub>3</sub>, with slightly tilted octahedra. Interesting, both β-CsPbI<sub>3</sub> and

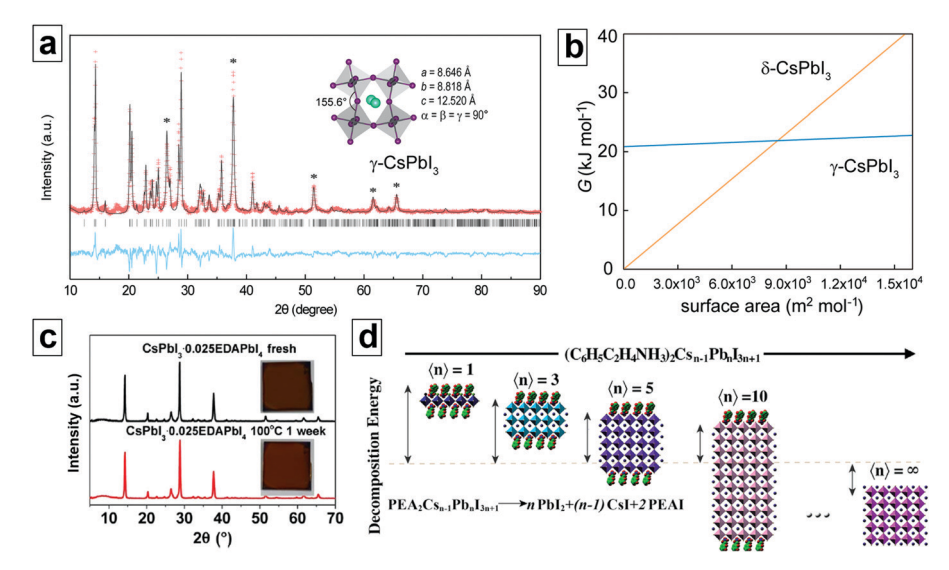


Fig. 8 (a) Rietveld refinement of the XRD pattern of the as-synthesized orthorhombic  $\gamma$ -CsPbl<sub>3</sub> perovskite, showing a space group of *Pbnm*. (b) Calculated Gibbs free energy of  $\gamma$ -CsPbI<sub>3</sub> and  $\alpha$ -CsPbI<sub>3</sub> polymorphs relative to bulk  $\delta$ -CsPbI<sub>3</sub> as a function of surface area using DFT. Adapted from ref. 95 with permission requested from ACS. (c) XRD patterns of CsPbl<sub>3</sub>·0.025EDAPbl<sub>4</sub> before and after storage under environmental conditions (100 °C, dry air) demonstrating its good stability. Adapted from ref. 96 with permission under a Creative Commons License. (d) Schematic illustration of the crystal structures of  $PEA_2Cs_{n-1}Pb_nX_{3n+1}$  with various n values. The relative decomposition energies of the  $PEA_2Cs_{n-1}Pb_nX_{3n+1}$  crystals based on DFT calculations are also shown. Adapted from ref. 97 with permission requested from Elsevier.

γ-CsPbI<sub>3</sub> have been claimed to show better stability than  $\alpha$ -CsPbI<sub>3</sub>. <sup>95,98,99</sup> Syntheses of β- and  $\gamma$ -CsPbI<sub>3</sub> perovskites can be enabled through incorporating suitable additives or dopants in the solution processes. 83,95 In a very recent study, Zhao et al. 95 have shown that a small amount of H2O addition in the CsPbI<sub>3</sub> precursor solutions facilitates direct crystallization of CsPbI<sub>3</sub> perovskite thin films in the  $\gamma$ -phase instead of the α-phase. As shown in Fig. 8a, the crystal structure of the γ-CsPbI<sub>3</sub> polymorph is confirmed based on the Rietveld refinement of the XRD pattern. The  $\gamma$ -CsPbI<sub>3</sub> crystal exhibits a space group of *Pbnm* (lattice parameters: a = 8.646 Å, b = 8.818 Å,  $c = 12.520 \text{ Å}, \alpha = \beta = \gamma = 90^{\circ}$ ). In Fig. 8b, the calculated Gibbs free energy relative to the bulk δ-CsPbI<sub>3</sub> as a function of surface area (linear relationship) using density functional theory (DFT) is plotted. The line slope indicates the surface free energy. The bulk free energy difference (when the surface area is zero) of  $\gamma$ -CsPbI<sub>3</sub> to δ-CsPbI<sub>3</sub> is 20.9 kJ mol<sup>-1</sup>. From Fig. 8b, Zhao *et al.* 95 have shown that when the surface area is greater than  $\sim 8600 \text{ m}^2 \text{ mol}^{-1}$ (corresponding to a film with roughly 100 nm grain size), γ-CsPbI<sub>3</sub> starts to show a lower Gibbs free energy than  $\delta$ -CsPbI<sub>3</sub>, suggesting a relatively higher phase stability. By tuning the added amount of  $H_2O$ , they have successfully prepared phase-pure  $\gamma$ -CsPbI<sub>3</sub> thin films with ~100 nm grain size in ambient conditions, which show a high PCE over 11%. Impressively, almost no efficiency loss is observed when the unencapsulated device is stored in the ambient environment for months or after continuous device operation under one-sun illumination for hours in the ambient environment. In the future, other synthetic methods such as pressure-assisted annealing may be employed to form new γ-CsPbI<sub>3</sub> thin films. It is also promising to synthesize surfacefunctionalized or doped γ-CsPbI<sub>3</sub> thin films, which could be even more stable.

The crystal dimensionality of CsPbI3 can be altered through incorporation of large organic cations into the crystal structure (instead of on the crystal surface), forming layered Ruddlesdon-Popper or Dion-Jacobson halide perovskite phases, so-called 'quasi-2D' perovskites. This is similar to the case of HHPs. 100 Note that the terminology of 'quasi-2D' or '2D' was adopted in the related original studies and thus used in the discussion here, although such terminology may not be appropriate. The 'quasi-2D' approach has early been utilized to stabilize the α-CsPbI<sub>3</sub> perovskite for red-color LEDs. 101 Here, the 1-naphthylmethylamine cation is introduced to form 'quasi-2D' perovskites, contributing to LEDs with a high external quantum efficiency of 3.7% and luminance of  $\sim 440$  cd m<sup>-2</sup>. This dimension-engineering method has also been introduced for stabilizing bulk CsPbI<sub>3</sub> perovskite thin films for PV applications. Liao et al. 102 have shown that BA cations added into CsPbI3 perovskite precursors form a 'quasi-2D' BA2CsPb2I7 perovskite, which exhibits a low crystallization temperature (  $\sim$  100  $^{\circ}$ C) and enhanced phase stability against humidity and heat. However, the crystal structure of BA2CsPb2I7 has not been fully studied in this study and thus it remains unclear whether BA2CsPb2I7 is a single-phase composition. The PSCs made using BA<sub>2</sub>CsPb<sub>2</sub>I<sub>7</sub> exhibit a PCE that is lower than 5%, which could be related to the low phase-purity. In a more promising approach by Zhang et al., 96 a 'quasi-2D' CsPbI3-based perovskite can be also formed by incorporation of divalent ethylenediaminium or butylenediaminium lead iodides in CsPbI<sub>3</sub> perovskite thin films, which leads to very promising film stability for more than one week under environmental conditions (100 °C, dry air), as revealed in Fig. 8c. These new 'quasi-2D' CsPbI<sub>3</sub>-based PSCs show stable PCEs up to 11.8%. In a later study, Jiang et al. 97 have systematically mixed PEAI of controlled amounts in the CsPbI3 precursor

solution, and claimed the formation of 'quasi-2D'  $PEA_2Cs_{n-1}Pb_nI_{3n+1}$ perovskites with various n values from 1 to  $\infty$ . A similar approach using the PEA+ cation is also reported by Li et al. 103 Such crystal-dimensionality engineering could be combined with the X-site anion alloying method, contributing to even more impressive perovskite stability. Jiang et al. have shown the PSC device made using the quasi-2D  $PEA_2Cs_{n-1}Pb_n(I_{2/3}Br_{1/3})_{3n+1}$ perovskite with an optimal n value of 40 exhibits a high PCE exceeding 11%, which has a retention of 93% after 40 days storage (unencapsulated) in ambient conditions. Regardless of the great device performance and stability, one may keep in mind that single-phase high-member Ruddlesdon-Popper phases are generally very difficult to synthesize due to the thermodynamic limit. 104 The exact composition and microstructure of the  $PEA_2Cs_{n-1}Pb_n(I_{2/3}Br_{1/3})_{3n+1}$  (n = 40) perovskite in Fig. 8d will need to be further confirmed. It is highly possible that when n > 5, instead of 'quasi-2D' perovskite phases, the perovskite thin films may consist of CsPbI<sub>3</sub> perovskite grains that are functionalized by PEA<sup>+</sup>, thus leading to the apparently enhanced stability. In addition, Zhang et al. 96 have also found that in these 'quasi-2D' CsPbI<sub>3</sub> perovskites, the grain size is usually smaller, which could be another contributing factor to the observed stability. Moreover, the exact crystal symmetry of these claimed 'quasi-2D' CsPbI<sub>3</sub> perovskites has not been revealed. It is envisioned that a systematic study on the effects of the organic-cation type on both crystal dimensionality and symmetry in CsPbI3 will help discover new phases of stable 'quasi-2D' CsPbI3 perovskites.

#### 3.6. Defect and microstructure engineering

Regardless of the high defect tolerance of IHPs in terms of optoelectronic properties, a high concentration of defects (e.g. vacancies, grain boundaries, pinholes) allows fast diffusion of ionic and molecular species within IHPs, affecting the longterm chemical stability. In this context, controlling the defects and microstructures in IHPs becomes important, which can be achieved with new processing methods. In a very recent study, Chen et al. 109 have showed a new route to make CsPbI2Br IHP thin films. They have applied gradient thermal annealing to control the grain growth, and then treated as-crystallized thin films with isopropanol antisolvent. This method leads to CsPbI<sub>2</sub>Br thin films with very low defect densities and thus excellent tolerance of the CsPbI2Br PSC devices to moisture and oxygen (90% of the initial PCE after aging for 120 h under 100 mW cm<sup>-2</sup> UV irradiation). In another study, Zhu et al. 110 have reported an 'intermolecular-exchange' method for CsPbIBr<sub>2</sub> films, where a CsPbIBr2 thin film deposited using the conventional 'one-step' method was post-reacted with a sequentiallydeposited CsI layer. The resulting thin film shows no pinholes, a very low density of grain boundaries, and high crystallinity. PSCs (carbon-electrode) using this thin film yield PCEs up to 9.16% with long-term stability (without encapsulation; 90% of the initial PCE after 60 days storage in 45% RH at 25 °C). Several other methods such as solvent-controlled growth, 106 flash annealing,111 dual-source vapor deposition112 and precursor solution engineering<sup>113-115</sup> are also demonstrated to fabricate

defect-less IHP thin films for stable high-performance IHP solar cells and LEDs. It is expected that accurate manipulation of defects and microstructures in IHPs will complement the other stabilization methods as mentioned before. However, there is still a lack of mechanistic understanding of the exact role of various types of defects and microstructures in the chemical stability of IHPs, calling for theoretical-experimental coupled effort in the future.

# 4. Stabilization of lead-free inorganic halide perovskites

The development of lead-free IHPs is still in its infancy stage. Especially in PV applications, lead-free IHP based PSCs usually exhibit very low PCEs. 46 The other applications of lead-free IHPs such as LEDs and photodetectors are just being developed. 116,117 But the restriction of lead use in future devices is not trivial, and there is a pressing need to develop stable lead-free perovskite materials for PV and optoelectronic applications. The following discussion will have a focus on reviewing previous efforts in stabilizing the lead-free CsSnI<sub>3</sub> perovskite, which has been the most popularly studied. The reported methods that show great promise are grain encapsulation, native-oxide surface passivation, and B-site cation replacement.

#### 4.1. Grain encapsulation

The lead-free CsSnI<sub>3</sub> compound has two polymorphs at ambient temperature: the black γ-CsSnI<sub>3</sub> perovskite (space group *Pnma*; a = 8.6885 Å, b = 8.7182 Å, c = 6.1908 Å) and the yellow δ-CsSnI<sub>3</sub> nonperovskite (space group *Pnma*; a = 10.350 Å,  $b = 4.7632 \text{ Å}, c = 17.684 \text{ Å}).^{120} \text{ More severely, the Sn}^{2+} \text{ in CsSnI}_{3}$ is very sensitive to oxygen in ambient conditions, and easily gets oxidized to Sn<sup>4+</sup>, forming Cs<sub>2</sub>SnI<sub>6</sub> with a double-perovskite structure (space group  $Fm\bar{3}m$ ; a = 11.65 Å). Although Cs<sub>2</sub>SnI<sub>6</sub> has a favorable bandgap of ~1.6 eV, it doesn't show good PV properties due to the low intrinsic deep-level defects. 119 Degradation of the γ-CsSnI<sub>3</sub> perovskite occurs via either first conversion to δ-CsSnI<sub>3</sub> and then Cs<sub>2</sub>SnI<sub>6</sub>, or direct conversion to Cs<sub>2</sub>SnI<sub>6</sub>. This has been schematically shown in Fig. 9a. The latter mechanism appears to be the case for thin films, 121,122 although the underlying reason remains unclear.

To prevent Sn2+ oxidation, Marshall et al.107 have used a SnCl<sub>2</sub> additive in the solution processing of γ-CsSnI<sub>3</sub> thin films. As illustrated in Fig. 9b and c, the resulting thin film contains γ-CsSnI<sub>3</sub> grains with SnCl<sub>2</sub> encapsulation layers (on film surfaces, at grain boundaries, or at pinholes). Fig. 9d and e compare the absorption spectra evolution of the SnCl2-free and SnCl2encapsulated CsSnI3 perovskite thin films with an increase of the exposure time to ambient air. The reduction in the film absorbance (e.g. at 500 nm) slowed down significantly once the SnCl<sub>2</sub> additive is added. SnF<sub>2</sub><sup>123</sup> and SnI<sub>2</sub> additives<sup>124</sup> have been also reported to stabilize CsSnI<sub>3</sub> PSCs, which may work under similar mechanisms. However, Marshall et al. 107 have also performed a systematic study on the effect of tin halides (i.e.  $SnF_2$ ,  $SnCl_2$ ,  $SnI_2$ ,  $SnBr_2$ ) on the  $\gamma$ -CsSnI<sub>3</sub> stabilization.

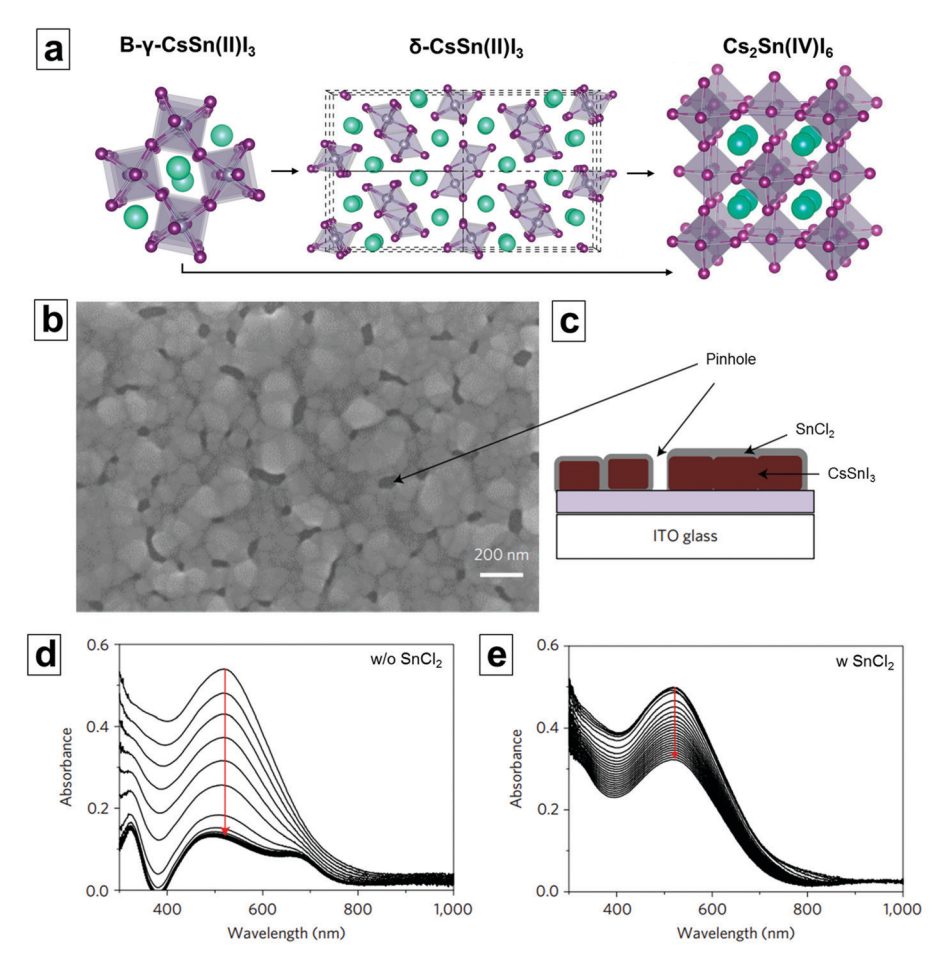


Fig. 9 (a) Schematic illustration showing the phase conversion of the  $\gamma$ -CsSnI<sub>3</sub> perovskite to the  $\delta$ -CsSnI<sub>3</sub> nonperovskite and Cs<sub>2</sub>SnI<sub>6</sub> double-perovskite. Adapted from ref. 118 with permission requested from the American Physical Society (APS). (b) Top-view SEM image and (c) schematic illustration of the  $SnCl_2$ -encapsulated  $CsSnl_3$  perovskite thin film. Evolution of UV-vis absorption spectra of (d) the  $SnCl_2$ -free and (e)  $SnCl_2$ -encapsulated  $CsSnl_3$  perovskite thin films with an increase in the exposure time to ambient air. Adapted from ref. 107 with permission requested from Nature Publishing Group.

While all tin halides show positive effects, SnCl2 is claimed to be the best for the following reasons: (i) Cl does not replace/ exchange I in the γ-CsSnI<sub>3</sub> crystal structure, making SnCl<sub>2</sub> easily aggregate on the grain surfaces; and (ii) SnCl<sub>2</sub> is much more soluble than SnF<sub>2</sub>. In this context, the stability of SnCl<sub>2</sub>incorporated CsSnI<sub>3</sub> PSCs (hole-transporting-layer-free) is claimed to be comparable to these lead-based PSCs with the same device architecture when tested in ambient air at 50 °C under continuous light illumination.

Although the grain-encapsulation method via additives has shown its promise, one of the major challenges associated with this method is the difficulty in achieving full encapsulation of grains with continuous stable secondary phases. Although previous reports have shown the possibility of full grain encapsulation for lead-containing HHP thin films, 125-127 suitable additives need to be developed for the CsSnI<sub>3</sub> perovskite. In this context, one promising direction is to tailor the chemical properties of additives and perform more accurate engineering of CsSnI<sub>3</sub> grain microstructures. The grain-encapsulation layer itself can be further chemically engineered with more antioxidant properties. Such effort may lead to more stable and efficient lead-free CsSnI<sub>3</sub> PSCs.

#### 4.2. Native-oxide surface passivation

Recently, Chen et al. 108 have shown a unique approach of 'native-oxide passivation' for stabilizing CsSnI3 based perovskite thin films. In this method, ultra-sensitive Ge is incorporated in the CsSnI<sub>3</sub> crystal structure, forming CsSn<sub>x</sub>Ge<sub>1-x</sub>I<sub>3</sub> perovskite alloys. Such alloys are ultra-sensitive to ambient air due to the existence of Ge. As shown in Fig. 10a, immediately upon the film being exposed to ambient air, a dense surface layer of GeO2 native oxide is formed on the CsSnxGe1-xI3 perovskite thin film, which protects the film bulk from further oxidation. In this work, Chen et al. have demonstrated the CsSn<sub>0.5</sub>Ge<sub>0.5</sub>I<sub>3</sub> composition as the proof of concept. It has been shown that the Goldschmidt tolerance ( $\sim 0.94$ ) and octahedral ( $\sim 0.4$ ) factors in CsSn<sub>0.5</sub>Ge<sub>0.5</sub>I<sub>3</sub> are also ideal for the structural stability of the CsSn<sub>x</sub>Ge<sub>1-x</sub>I<sub>3</sub> alloy crystal in addition to nativeoxide passivation. The chemical stability of the CsSn<sub>0.5</sub>Ge<sub>0.5</sub>I<sub>3</sub> perovskite thin film is compared with the CsSnI<sub>3</sub> IHP, the CsPbI<sub>3</sub> IHP, and the prototypical MAPbI<sub>3</sub> HHP by monitoring the intensity of the characteristic XRD peak of each phase. It can be seen in Fig. 10b that the CsSn<sub>0.5</sub>Ge<sub>0.5</sub>I<sub>3</sub> perovskite retains its phase after exposure to environmental conditions

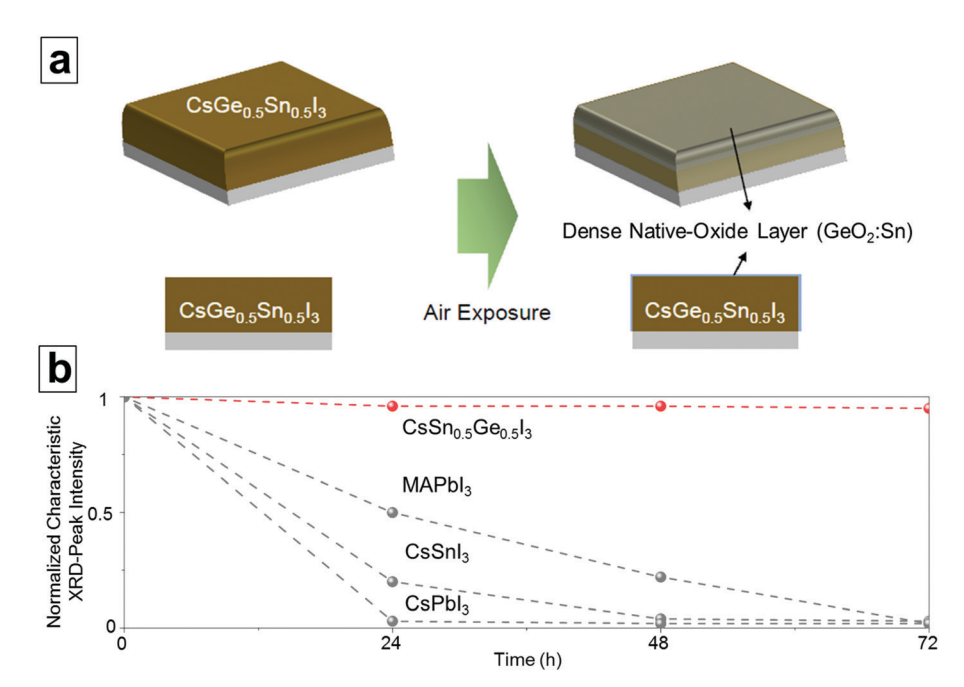


Fig. 10 (a) Schematic illustration of the CsSn<sub>0.5</sub>Ge<sub>0.5</sub>I<sub>3</sub> perovskite thin film, which immediately forms a dense surface layer of native oxide (Sn-doped GeO<sub>2</sub>) upon air exposure. This surface layer stabilizes the film effectively. (b) Monitoring the intensity variation of the characteristic XRD peak of the CsSn<sub>0.5</sub>Ge<sub>0.5</sub>I<sub>3</sub>, CsSnI<sub>3</sub>, MAPbI<sub>3</sub>, and CsPbI<sub>3</sub> thin films with an increase of the exposure time to ambient conditions. Adapted from ref. 108 with permission under the Creative Commons Attribution 4.0 International License

(45 °C, 80% RH) for 72 h, showing significantly better stability than CsSnI<sub>3</sub>, CsPbI<sub>3</sub>, and even MAPbI<sub>3</sub>. Regarding the device performance and stability, CsSn<sub>0.5</sub>Ge<sub>0.5</sub>I<sub>3</sub> PSCs show a maximum PCE of 7.11% and a stabilized PCE output of 7.03%. After 500 h continuous operation in a dry nitrogen atmosphere under onesun-intensity illumination, 93% of the initial PCE can be retained. Regarding the device stability in air, the CsSn<sub>0.5</sub>Ge<sub>0.5</sub>I<sub>3</sub> PSC shows 91% retention of the initial PCE after the device is stored for 100 h under one-sun-intensity illumination. This is the best stability of all lead-free perovskite PSCs reported to date.

Native-oxide passivation represents a new direction for stabilizing the lead-free CsSnI<sub>3</sub> perovskite. Nevertheless, further improvement would be required. For example, GeO2 is still relatively hydrophilic, 128 which renders the surface layer not stable in a humid environment. It may be worthwhile to explore other alternative elements that could replace Ge and form more hydrophobic native-oxide surface layers. This concept may be generic for stabilizing a variety of lead-free IHPs that are not limited to CsSnI<sub>3</sub>.

#### 4.3. New IHPs with stable B-site cations

The stability of CsSnI<sub>3</sub> can be mitigated via replacement of the unstable Sn<sup>2+</sup> with other stable metal cations. The B-site cation replacement can lead to different crystal structures with different chemical formulas depending on the valence states of the B-site cation. Bi<sup>3+</sup> and Sb<sup>3+</sup> have been used to form crystals with a chemical formula of A<sub>3</sub>B<sub>2</sub>X<sub>9</sub>. However, this reduces the crystal dimensionality from 3D to 1D, leading to significantly increased bandgaps and anisotropic properties which are not favorable for solar cell applications. 129

In this context, metal cations with +4 oxidation states are explored for B-site replacement, forming special vacancy-ordered double perovskites with A2BX6 compositions. Ju et al.46 have reported a new family of vacancy-ordered double perovskites  $Cs_2TiX_6$ , X = I<sup>-</sup>, Br<sup>-</sup>, or Cl<sup>-</sup>, based on chemically stable titanium(w) as the B-site cation. Ti is in its +4 oxidation state in Cs2TiX6, making this compound chemically resist further oxidation. The stability of the Cs2TiX6 series has shown clear advantages over HHP compounds with similar bandgaps, which has been proved experimentally. In a parallel study by Chen et al., 130 a thin film of Cs<sub>2</sub>TiBr<sub>6</sub> is processed using a two-step vapor-deposition method. Excellent optoelectronic properties (long carrier diffusion lengths of > 100 nm) have been measured in ambient conditions, which could be partially attributed to its high chemical stability. Note that for air-sensitive CsSnI<sub>3</sub> perovskites, good optoelectronic properties could be only measured under a vacuum. The stability of Cs2TiBr6 thin films is tested by applying thermal (200 °C, 6 h, N2 atmosphere), light (one-sun, encapsulated), and moisture (23 °C, 80% RH, 6 h) stresses; no degradation is observed and the Cs<sub>2</sub>TiBr<sub>6</sub> PSC shows stable performance (only 6% decay of the initial PCE) after storage in environmental conditions (70 °C, 30% RH, ambient light). Palladium (Pd4+) is another alternative B-site cation, which is reported by Sakai et al., 131 although Pd is a relatively expensive metal. The resulting Cs<sub>2</sub>PbBr<sub>6</sub> double-perovskite compound exhibits good photoluminescence properties and a favorable band gap of 1.6 eV. Like Cs<sub>2</sub>TiBr<sub>6</sub>, very strong water-resistance is observed for Cs<sub>2</sub>PdBr<sub>6</sub>. Pd is also in its stable +4 oxidation state in Cs<sub>2</sub>PdBr<sub>6</sub>, which renders this material in principle not oxygen-sensitive. Nevertheless, Cs2PdBr6-based PSCs have not

been reported until now. Another possible method for B-site cation replacement is to form regular double perovskites of A<sub>2</sub>B'B"X<sub>6</sub>, where B' and B" are in their +1 and +3 oxidation states, respectively. Possible compounds may include, but are not limited to, Cs2AgBiX6 and Cs2AgInX6. Especially the Cs<sub>2</sub>AgBiBr<sub>6</sub> double-perovskite has been reported with a long photoluminescence lifetime of 660 ns at room temperature, and it is significantly more thermal- and moisture-stable than the MAPbI<sub>3</sub> HHP. One demerit of Cs<sub>2</sub>AgBiBr<sub>6</sub> is that this compound exhibits a relatively large bandgap of 1.91 eV. 132 Although exchanging I with Br in Cs<sub>2</sub>AgBiBr<sub>6</sub> invariably reduces the bandgap, Cs<sub>2</sub>AgBiI<sub>6</sub> has been predicted to be thermodynamically unstable in the bulk, and thus, no successful synthesis of bulk Cs<sub>2</sub>AgBiI<sub>6</sub> crystals or thin films has been reported.<sup>133</sup> Promisingly, Creutze et al. 134 show that Cs<sub>2</sub>AgBiI<sub>6</sub> phases could be made in nanocrystals via an anion-exchange process starting from Cs<sub>2</sub>AgBiBr<sub>6</sub>. The successful stabilization of Cs<sub>2</sub>AgBiI<sub>6</sub> in nanocrystals is similar to the case of α-CsPbI3 as discussed in Section 3.2. This nanocrystal approach opens up a new possibility to synthesize or stabilize new lead-free IHPs that are considered as unstable or non-existing in the bulk.

## Summary and perspectives

IHPs completely eliminate the instability issues associated with volatile and hygroscopic organic cations in their hybrid organicinorganic counterparts, offering the promise of relatively high intrinsic or thermodynamic stability against decomposition to the binary halide products. Nevertheless, many of the important IHPs (e.g. CsPbI<sub>3</sub>, CsSnI<sub>3</sub>) still suffer from severe chemical degradation under environmental conditions, which is mostly caused by either polymorphic transformation, oxidation, or their combination. While the reported stabilization protocols as reviewed above provide feasible solutions to mitigate this outstanding issue to some extent, we envision that the following research directions could be of great importance for further enhancing the stability of IHP materials and devices:

- (i) Revealing the exact degradation mechanisms of IHPs via in situ characterization. Advanced synchrotron-based<sup>135</sup> and TEM-based characterization 136 may find great use here as these techniques offer desirable resolution for understanding nanoscale materials/device behaviors. Roles of ion-types, defects (interstitials and vacancies), crystal morphologies, and microstructures (grain boundaries, orientation, etc.) in the IHP degradation processes could be understood through a combination of conventional and in situ characterization. There have been some pioneering in situ studies revealing the degradation mechanism of HHPs. 137 Similar methods could be applied to IHPs for probing the degradation mechanisms of IHPs (oxidation and polymorphic transition) which are usually different from those (hydration and decomposition) for HHPs.
- (ii) Precise tailoring of the compositions/microstructures of IHP thin films at the nanoscale. This should be guided by the valuable inputs from in situ and high-resolution diagnostics of the IHP degradation. Continuous grain-boundary functionalization 126

using chemically-engineered additives is one promising direction, which will provide a complete encapsulation layer for individual grains in thin films, leading to the most reliable protection. Furthermore, new stabilization methods can be invented by integrating several established methods (additives, nanocrystals, surface/grain boundary functionalization, etc.).

- (iii) Rational design and synthesis of new stable IHP materials with the aid of high-throughput computational screening processes. The previous research in this direction has led to the discovery of some good perovskite materials (e.g. Cs<sub>2</sub>TiX<sub>6</sub>) potentially with more desired features such as less-toxicity and more ideal bandgaps. In the future, artificial intelligence processes will be required to be developed for rapid prediction of new stable IHP materials that are suitable for optoelectronic applications.
- (iv) Design of novel architectures for IHP optoelectronics. Some studies have shown fabrication of new IHP-ETL or IHP-HTL interfaces (e.g. MoO<sub>x</sub>-CsPbIBr<sub>2</sub>, 138 ZnO/C60-CsPbI<sub>2</sub>Br<sup>59</sup>) and electrode materials (e.g. carbon<sup>139</sup>) that not only allow better charge extraction, but also provide device encapsulation function. But this direction has still been much less explored for IHPs compared with that for HHPs. Therefore, more effort in understanding the surfaces and interfaces of IHPs as well as the degradation of IHPs at the device scale will accelerate the innovation of new IHP device structures where IHPs are highly stabilized.

### Conflicts of interest

There are no conflicts to declare.

# Acknowledgements

Y. Zhou is thankful for funding support from the US National Science Foundation (grant no. OIA-1538893). Y. Zhao acknowledges support from the National Natural Science Foundation of China (grant no. 51861145101 and 21777096).

#### References

- 1 M. A. Green, A. Ho-Baillie and H. J. Snaith, Nat. Photonics, 2014, 8, 506-514.
- 2 W. Li, Z. Wang, F. Deschler, S. Gao, R. H. Friend and A. K. Cheetham, Nat. Rev. Mater., 2017, 16099, DOI: 10.1038/natrevmats.2016.99.
- 3 Y. Zhao and K. Zhu, Chem. Soc. Rev., 2016, 45, 655-689.
- 4 N.-G. Park, M. Grätzel, T. Miyasaka, K. Zhu and K. Emery, Nat. Energy, 2016, 1, 16152.
- 5 A. Kojima, K. Teshima, Y. Shirai and T. Miyasaka, J. Am. Chem. Soc., 2009, 131, 6050-6051.
- 6 I. Chung, B. Lee, J. He, R. P. H. Chang and M. G. Kanatzidis, Nature, 2012, 485, 486-489.
- 7 H.-S. Kim, C.-R. Lee, J.-H. Im, K.-B. Lee, T. Moehl, A. Marchioro, S.-J. Moon, R. Humphry-Baker, J.-H. Yum, J. E. Moser, M. Gratzel and N.-G. Park, Sci. Rep., 2012, 2, 1-7.

- 8 Q. Dong, Y. Fang, Y. Shao, P. Mulligan, J. Qiu, L. Cao and J. Huang, *Science*, 2015, 347, 967–970.
- 9 S. D. Stranks, G. E. Eperon, G. Grancini, C. Menelaou, M. J. P. Alcocer, T. Leijtens, L. M. Herz, A. Petrozza and H. J. Snaith, *Science*, 2013, 342, 341–344.
- 10 J. H. Noh, S. H. Im, J. H. Heo, T. N. Mandal and S. I. Seok, Nano Lett., 2013, 13, 1764–1769.
- 11 K. X. Steirer, P. Schulz, G. Teeter, V. Stevanovic, M. Yang, K. Zhu and J. J. Berry, *ACS Energy Lett.*, 2016, 1, 360–366.
- 12 J. Kang and L.-W. Wang, J. Phys. Chem. Lett., 2017, 8, 489-493.
- 13 M. V. Kovalenko, L. Protesescu and M. I. Bodnarchuk, *Science*, 2017, 358, 745–750.
- 14 H. Wei, Y. Fang, P. Mulligan, W. Chuirazzi, H.-H. Fang, C. Wang, B. R. Ecker, Y. Gao, M. A. Loi, L. Cao and J. Huang, *Nat. Photonics*, 2016, 10, 333–340.
- 15 W. Pan, H. Wu, J. Luo, Z. Deng, C. Ge, C. Chen, X. Jiang, W.-J. Yin, G. Niu, L. Zhu, L. Yin, Y. Zhou, Q. Xie, X. Ke, M. Sui and J. Tang, *Nat. Photonics*, 2017, 11, 726–732.
- 16 Z.-K. Tan, R. S. Moghaddam, M. L. Lai, P. Docampo, R. Higler, F. Deschler, M. Price, A. Sadhanala, L. M. Pazos, D. Credgington, F. Hanusch, T. Bein, H. J. Snaith and R. H. Friend, *Nat. Nanotechnol.*, 2014, 9, 687–692.
- 17 N. Wang, L. Cheng, R. Ge, S. Zhang, Y. Miao, W. Zou, C. Yi, Y. Sun, Y. Cao, R. Yang, Y. Wei, Q. Guo, Y. Ke, M. Yu, Y. Jin, Y. Liu, Q. Ding, D. Di, L. Yang, G. Xing, H. Tian, C. Jin, F. Gao, R. H. Friend, J. Wang and W. Huang, *Nat. Photonics*, 2016, 10, 699–704.
- 18 https://www.nrel.gov/pv/assets/pdfs/pv-efficiencies-07-17-2018.pdf.
- 19 Z. Cheng and J. Lin, CrystEngComm, 2010, 12, 2646.
- 20 W. A. Dunlap-Shohl, Y. Zhou, N. P. Padture and D. B. Mitzi, Chem. Rev., 2018, DOI: 10.1021/acs.chemrev.8b00318.
- 21 W. Travis, E. N. K. Glover, H. Bronstein, D. O. Scanlon and R. G. Palgrave, *Chem. Sci.*, 2016, 7, 4548–4556.
- 22 C. C. Stoumpos, D. H. Cao, D. J. Clark, J. Young, J. M. Rondinelli, J. I. Jang, J. T. Hupp and M. G. Kanatzidis, *Chem. Mater.*, 2016, **28**, 2852–2867.
- 23 P. Yang, G. Liu, B. Liu, X. Liu, Y. Lou, J. Chen and Y. Zhao, Chem. Commun., 2018, 54, 11638–11641.
- 24 T. Zhang, Y. Hui, L. Chen, G. Li, B. Mao and Y. Zhao, J. Phys. D: Appl. Phys., 2018, 51, 404001.
- 25 L. Mao, W. Ke, L. Pedesseau, Y. Wu, C. Katan, J. Even, M. R. Wasielewski, C. C. Stoumpos and M. G. Kanatzidis, J. Am. Chem. Soc., 2018, 140, 3775–3783.
- 26 B.-W. Park, B. Philippe, X. Zhang, H. Rensmo, G. Boschloo and E. M. J. Johansson, *Adv. Mater.*, 2015, 27, 6806–6813.
- 27 Y. Lou, M. Fang, J. Chen and Y. Zhao, *Chem. Commun.*, 2018, 54, 3779–3782.
- 28 M. G. Ju, M. Chen, Y. Y. Zhou, H. F. Garces, J. Dai, L. Ma, N. P. Padture and X. C. Zeng, ACS Energy Lett., 2018, 3, 297–304.
- 29 M. I. Saidaminov, J. Almutlaq, S. Sarmah, I. Dursun, A. A. Zhumekenov, R. Begum, J. Pan, N. Cho, O. F. Mohammed and O. M. Bakr, *ACS Energy Lett.*, 2016, 1, 840–845.
- 30 M.-G. Ju, J. Dai, L. Ma, Y. Zhou and X. C. Zeng, *J. Am. Chem. Soc.*, 2018, **140**, 10456–10463.

- 31 D. Zhang, Y. Zhu, L. Liu, X. Ying, C.-E. Hsiung, R. Sougrat, K. Li and Y. Han, *Science*, 2018, 359, 675–679.
- 32 Y. Yu, D. D. Zhang, C. Kisielowski, L. T. Dou, N. Kornienko, Y. Bekenstein, A. B. Wong, A. P. Alivisatos and P. D. Yang, *Nano Lett.*, 2016, **16**, 7530–7535.
- 33 Y. Zhou and K. Zhu, ACS Energy Lett., 2016, 1, 64-67.
- 34 S.-H. Turren-Cruz, A. Hagfeldt and M. Saliba, *Science*, 2018, 362, 449–453.
- 35 W. Chen, Y. Wu, Y. Yue, J. Liu, W. Zhang, X. Yang, H. Chen, E. Bi, I. Ashraful, M. Grätzel and L. Han, *Science*, 2015, 350, 944–948.
- 36 E. M. Sanehira, A. R. Marshall, J. A. Christians, S. P. Harvey, P. N. Ciesielski, L. M. Wheeler, P. Schulz, L. Y. Lin, M. C. Beard and J. M. Luther, Sci. Adv., 2017, 3, eaao4204.
- 37 A. Swarnkar, A. R. Marshall, E. M. Sanehira, B. D. Chernomordik, D. T. Moore, J. A. Christians, T. Chakrabarti and J. M. Luther, *Science*, 2016, 354, 92–95.
- 38 R. E. Beal, D. J. Slotcavage, T. Leijtens, A. R. Bowring, R. A. Belisle, W. H. Nguyen, G. F. Burkhard, E. T. Hoke and M. D. McGehee, *J. Phys. Chem. Lett.*, 2016, 7, 746–751.
- 39 W. K. Zhou, Y. C. Zhao, X. Zhou, R. Fu, Q. Li, Y. Zhao, K. H. Liu, D. P. Yu and Q. Zhao, J. Phys. Chem. Lett., 2017, 8, 4122–4128.
- 40 Y. Y. Zhang, S. Y. Chen, P. Xu, H. Xiang, X. G. Gong, A. Walsh and S. H. Wei, *Chin. Phys. Lett.*, 2018, 35, 6.
- 41 B. Conings, J. Drijkoningen, N. Gauquelin, A. Babayigit, J. D'Haen, L. D'Olieslaeger, A. Ethirajan, J. Verbeeck, J. Manca, E. Mosconi, F. De Angelis and H.-G. Boyen, Adv. Energy Mater., 2015, 5, 1500477.
- 42 G. P. Nagabhushana, R. Shivaramaiah and A. Navrotsky, *Proc. Natl. Acad. Sci. U. S. A.*, 2016, **113**, 7717–7721.
- 43 C. Y. Yi, J. S. Luo, S. Meloni, A. Boziki, N. Ashari-Astani, C. Gratzel, S. M. Zakeeruddin, U. Rothlisberger and M. Gratzel, *Energy Environ. Sci.*, 2016, 9, 656–662.
- 44 Z. Li, M. J. Yang, J. S. Park, S. H. Wei, J. J. Berry and K. Zhu, *Chem. Mater.*, 2016, **28**, 284–292.
- 45 M. Saliba, T. Matsui, J.-Y. Seo, K. Domanski, J.-P. Correa-Baena, M. K. Nazeeruddin, S. M. Zakeeruddin, W. Tress, A. Abate, A. Hagfeldt and M. Gratzel, *Energy Environ. Sci.*, 2016, 9, 1989–1997.
- 46 M.-G. Ju, M. Chen, Y. Zhou, J. Dai, L. Ma, N. P. Padture and X. C. Zeng, *Joule*, 2018, 2, 1231–1241.
- 47 N. Aristidou, I. Sanchez-Molina, T. Chotchuangchutchaval, M. Brown, L. Martinez, T. Rath and S. A. Haque, *Angew. Chem.*, *Int. Ed.*, 2015, 54, 8208–8212.
- 48 N. Aristidou, C. Eames, I. Sanchez-Molina, X. Bu, J. Kosco, M. S. Islam and S. A. Haque, *Nat. Commun.*, 2017, **8**, 15218.
- 49 J. Mizusaki, K. Arai and K. Fueki, Solid State Ionics, 1983, 11, 203–211.
- 50 D. Yang, W. Ming, H. Shi, L. Zhang and M.-H. Du, *Chem. Mater.*, 2016, 28, 4349–4357.
- 51 Y. Yuan and J. Huang, Acc. Chem. Res., 2016, 49, 286-293.
- 52 arXiv:1801.08519v2 [cond-mat.mtrl-sci].
- 53 W. Xiang, Z. Wang, D. J. Kubicki, W. Tress, J. Luo, D. Prochowicz, S. Akin, L. Emsley, J. Zhou, G. Dietler, M. Grätzel and A. Hagfeldt, *Joule*, 2019, 3, 205–214.

- 54 G. E. Eperon, G. M. Paterno, R. J. Sutton, A. Zampetti, A. A. Haghighirad, F. Cacialli and H. J. Snaith, J. Mater. Chem. A, 2015, 3, 19688-19695.
- 55 R. J. Sutton, G. E. Eperon, L. Miranda, E. S. Parrott, B. A. Kamino, J. B. Patel, M. T. Horantner, M. B. Johnston, A. A. Haghighirad, D. T. Moore and H. J. Snaith, Adv. Energy Mater., 2016, 6, 6.
- 56 G. Q. Tong, H. Li, D. T. Li, Z. F. Zhu, E. Z. Xu, G. P. Li, L. W. Yu, J. Xu and Y. Jiang, Small, 2018, 14, 1702523.
- 57 W. Ahmad, J. Khan, G. D. Niu and J. Tang, Sol. RRL, 2017, 1, 1700048.
- 58 H. N. Chen, S. S. Xiang, W. P. Li, H. C. Liu, L. Q. Zhu and S. H. Yang, Sol. RRL, 2018, 2, 23.
- 59 C. Liu, W. Z. Li, C. L. Zhang, Y. P. Ma, J. D. Fan and Y. H. Mai, J. Am. Chem. Soc., 2018, 140, 3825-3828.
- 60 C. Y. Chen, H. Y. Lin, K. M. Chiang, W. L. Tsai, Y. C. Huang, C. S. Tsao and H. W. Lin, Adv. Mater., 2017, 29, 8.
- 61 J. K. Nam, M. S. Jung, S. U. Chai, Y. J. Choi, D. Kim and J. H. Park, J. Phys. Chem. Lett., 2017, 8, 2936-2940.
- 62 Y. Wang, T. Zhang, F. Xu, Y. Li and Y. Zhao, Sol. RRL, 2018, 2, 1700180.
- 63 J. Liang, P. Zhao, C. Wang, Y. Wang, Y. Hu, G. Zhu, L. Ma, J. Liu and Z. Jin, J. Am. Chem. Soc., 2017, 139, 14009-14012.
- 64 F. Liu, C. Ding, Y. H. Zhang, T. S. Ripolles, T. Kamisaka, T. Toyoda, S. Hayase, T. Minemoto, K. Yoshino, S. Y. Dai, M. Yanagida, H. Noguchi and Q. Shen, J. Am. Chem. Soc., 2017, 139, 16708-16719.
- 65 Z. T. Du, D. F. Fu, T. Yang, Z. Fang, W. N. Liu, F. M. Gao, L. Wang, Z. B. Yang, J. Teng, H. Zhang and W. Y. Yang, J. Mater. Chem. C, 2018, 6, 6287–6296.
- 66 F. Yang, D. Hirotani, G. Kapil, M. A. Kamarudin, C. H. Ng, Y. H. Zhang, Q. Shen and S. Hayase, Angew. Chem., Int. Ed., 2018, 57, 12745-12749.
- 67 Y. Q. Hu, F. Bai, X. B. Liu, Q. M. Ji, X. L. Miao, T. Qiu and S. F. Zhang, ACS Energy Lett., 2017, 2, 2219-2227.
- 68 S. S. Xiang, W. P. Li, Y. Wei, J. M. Liu, H. C. Liu, L. Q. Zhu and H. N. Chen, Nanoscale, 2018, 10, 9996-10004.
- 69 A. K. Jena, A. Kulkarni, Y. Sanehira, M. Ikegami and T. Miyasaka, Chem. Mater., 2018, 30, 6668-6674.
- 70 Q. A. Akkerman, D. Meggiolaro, Z. Y. Dang, F. De Angelis and L. Manna, ACS Energy Lett., 2017, 2, 2183-2186.
- 71 D. L. Bai, J. R. Zhang, Z. W. Jin, H. Bian, K. Wang, H. R. Wang, L. Liang, Q. Wang and S. F. Liu, ACS Energy Lett., 2018, 3, 970.
- 72 L. Y. Huang and W. R. L. Lambrecht, Phys. Rev. B: Condens. Matter Mater. Phys., 2016, 93, 8.
- 73 G. Kieslich, S. Sun and A. K. Cheetham, Chem. Sci., 2015, 6, 3430-3433.
- 74 C. H. Yoder, Ionic Compounds: Applications of Chemistry to Mineralogy, John Wiley & Sons, Inc., 2006.
- 75 R. Shannon, Acta Crystallogr., 1976, 32, 751-767.
- 76 W. Ke, I. Spanopoulos, C. C. Stoumpos and M. G. Kanatzidis, Nat. Commun., 2018, 9, 4785.
- 77 J. Liang, Z. Liu, L. Qiu, Z. Hawash, L. Meng, Z. Wu, Y. Jiang, L. K. Ono and Y. Qi, Adv. Energy Mater., 2018, 8, 1800504.

- 78 C. C. Stoumpos, C. D. Malliakas and M. G. Kanatzidis, Inorg. Chem., 2013, 52, 9019-9038.
- 79 L. Protesescu, S. Yakunin, M. I. Bodnarchuk, F. Krieg, R. Caputo, C. H. Hendon, R. X. Yang, A. Walsh and M. V. Kovalenko, Nano Lett., 2015, 15, 3692-3696.
- 80 H. Yang, Y. Zhang, K. Hills-Kimball, Y. Zhou and O. Chen, Sustainable Energy Fuels, 2018, 2, 2381-2397.
- 81 J. Yuan, X. Ling, D. Yang, F. Li, S. Zhou, J. Shi, Y. Qian, J. Hu, Y. Sun, Y. Yang, X. Gao, S. Duhm, Q. Zhang and W. Ma, Joule, 2018, 2, 2450-2463.
- 82 Z. Zolfaghari, E. Hassanabadi, D. Pitarch-Tena, S. J. Yoon, Z. Shariatinia, J. van de Lagemaat, J. M. Luther and I. Mora-Seró, ACS Energy Lett., 2019, 4, 251-258.
- 83 Y. P. Fu, M. T. Rea, J. Chen, D. J. Morrow, M. P. Hautzinger, Y. Z. Zhao, D. X. Pan, L. H. Manger, J. C. Wright, R. H. Goldsmith and S. Jin, Chem. Mater., 2017, 29, 8385-8394.
- 84 B. Li, Y. A. Zhang, L. Fu, T. Yu, S. J. Zhou, L. Y. Zhang and L. W. Yin, Nat. Commun., 2018, 9, 1076.
- 85 Q. Wang, X. P. Zheng, Y. H. Deng, J. J. Zhao, Z. L. Chen and J. S. Huang, Joule, 2017, 1, 371-382.
- 86 B. Jeong, H. Han, Y. J. Choi, S. H. Cho, E. H. Kim, S. W. Lee, J. S. Kim, C. Park, D. Kim and C. Park, Adv. Funct. Mater., 2018, 28, 1706401.
- 87 S. Xiang, Z. Fu, W. Li, Y. Wei, J. Liu, H. Liu, L. Zhu, R. Zhang and H. Chen, ACS Energy Lett., 2018, 3, 1824-1831.
- 88 D. Y. Heo, S. M. Han, N. S. Woo, Y. J. Kim, T.-Y. Kim, Z. Luo and S. Y. Kim, J. Phys. Chem. C, 2018, 122, 15903-15910.
- 89 N. K. Noel, M. Congiu, A. J. Ramadan, S. Fearn, D. P. McMeekin, J. B. Patel, M. B. Johnston, B. Wenger and H. J. Snaith, Joule, 2017, 1, 328-343.
- 90 K. Wang, Z. Jin, L. Liang, H. Bian, D. Bai, H. Wang, J. Zhang, Q. Wang and S. Liu, Nat. Commun., 2018, 9, 4544.
- 91 Y. Wang, T. Zhang, M. Kan, Y. Li, T. Wang and Y. Zhao, Joule, 2018, 2, 2065-2075.
- 92 A. Dutta, S. K. Dutta, S. Das Adhikari and N. Pradhan, Angew. Chem., Int. Ed., 2018, 57, 9083-9087.
- 93 Y. Wang, T. Zhang, M. Kan and Y. Zhao, J. Am. Chem. Soc., 2018, 140, 12345-12348.
- 94 X. Ding, H. Chen, Y. Wu, S. Ma, S. Dai, S. Yang and J. Zhu, J. Mater. Chem. A, 2018, 6, 18258-18266.
- 95 B. Zhao, S.-F. Jin, S. Huang, N. Liu, J.-Y. Ma, D.-J. Xue, Q. Han, J. Ding, Q.-Q. Ge, Y. Feng and J.-S. Hu, J. Am. Chem. Soc., 2018, 140, 11716-11725.
- 96 T. Y. Zhang, M. I. Dar, G. Li, F. Xu, N. J. Guo, M. Gratzel and Y. X. Zhao, Sci. Adv., 2017, 3, e1700841.
- 97 Y. Jiang, J. Yuan, Y. Ni, J. Yang, Y. Wang, T. Jiu, M. Yuan and J. Chen, Joule, 2018, 2, 1356-1368.
- 98 R. J. Sutton, M. R. Filip, A. A. Haghighirad, N. Sakai, B. Wenger, F. Giustino and H. J. Snaith, ACS Energy Lett., 2018, 3, 1787-1794.
- 99 Y. Fu, M. T. Rea, J. Chen, D. J. Morrow, M. P. Hautzinger, Y. Zhao, D. Pan, L. H. Manger, J. C. Wright, R. H. Goldsmith and S. Jin, Chem. Mater., 2017, 29, 8385-8394.
- 100 Y. N. Chen, Y. Sun, J. J. Peng, J. H. Tang, K. B. Zheng and Z. Q. Liang, Adv. Mater., 2018, 30, 1703487.

- 101 S. T. Zhang, C. Yi, N. N. Wang, Y. Sun, W. Zou, Y. Q. Wei, Y. Cao, Y. F. Miao, R. Z. Li, Y. Yin, N. Zhao, J. P. Wang and W. Huang, *Adv. Mater.*, 2017, 29, 1606600.
- 102 J. F. Liao, H. S. Rao, B. X. Chen, D. B. Kuang and C. Y. Su, *J. Mater. Chem. A*, 2017, 5, 2066–2072.
- 103 F. M. Li, Y. H. Pei, F. Xiao, T. X. Zeng, Z. Yang, J. J. Xu, J. Sun, B. Peng and M. Z. Liu, *Nanoscale*, 2018, **10**, 6318–6322.
- 104 C. M. M. Soe, G. P. Nagabhushana, R. Shivaramaiah, H. Tsai, W. Nie, J.-C. Blancon, F. Melkonyan, D. H. Cao, B. Traoré, L. Pedesseau, M. Kepenekian, C. Katan, J. Even, T. J. Marks, A. Navrotsky, A. D. Mohite, C. C. Stoumpos and M. G. Kanatzidis, *Proc. Natl. Acad. Sci. U. S. A.*, 2019, 116, 58–66.
- 105 Q. Wang, X. Zheng, Y. Deng, J. Zhao, Z. Chen and J. Huang, Joule, 2017, 1, 371–382.
- 106 P. Wang, X. Zhang, Y. Zhou, Q. Jiang, Q. Ye, Z. Chu, X. Li, X. Yang, Z. Yin and J. You, *Nat. Commun.*, 2018, 9, 2225.
- 107 K. P. Marshall, M. Walker, R. I. Walton and R. A. Hatton, Nat. Energy, 2016, 1, 16178.
- 108 M. Chen, M.-G. Ju, H. F. Garces, A. D. Carl, L. K. Ono, Z. Hawash, Y. Zhang, T. Shen, Y. Qi, R. L. Grimm, D. Pacifici, X. C. Zeng, Y. Zhou and N. P. Padture, *Nat. Commun.*, 2019, 10, 16.
- 109 W. Chen, H. Chen, G. Xu, R. Xue, S. Wang, Y. Li and Y. Li, *Joule*, 2019, 3, 191–204.
- 110 W. Zhu, Q. Zhang, D. Chen, Z. Zhang, Z. Lin, J. Chang, J. Zhang, C. Zhang and Y. Hao, Adv. Energy Mater., 2018, 8, 1802080.
- 111 Y. Gao, Y. Dong, K. Huang, C. Zhang, B. Liu, S. Wang, J. Shi, H. Xie, H. Huang, S. Xiao, J. He, Y. Gao, R. A. Hatton and J. Yang, *ACS Photonics*, 2018, 5, 4104–4110.
- 112 Q. Ma, S. Huang, X. Wen, M. A. Green and A. W. Y. Ho-Baillie, *Adv. Energy Mater.*, 2016, **6**, 1502202.
- 113 F. Jin, B. Zhao, B. Chu, H. Zhao, Z. Su, W. Li and F. Zhu, J. Mater. Chem. C, 2018, 6, 1573-1578.
- 114 N. Yantara, S. Bhaumik, F. Yan, D. Sabba, H. A. Dewi, N. Mathews, P. P. Boix, H. V. Demir and S. Mhaisalkar, *J. Phys. Chem. Lett.*, 2015, **6**, 4360–4364.
- 115 D. Liu, C. Yang, M. Bates and R. R. Lunt, *iScience*, 2018, **6**, 272–279.
- 116 J. Luo, X. Wang, S. Li, J. Liu, Y. Guo, G. Niu, L. Yao, Y. Fu, L. Gao, Q. Dong, C. Zhao, M. Leng, F. Ma, W. Liang, L. Wang, S. Jin, J. Han, L. Zhang, J. Etheridge, J. Wang, Y. Yan, E. H. Sargent and J. Tang, *Nature*, 2018, 563, 541–545.
- 117 B. Yang, Y.-J. Li, Y.-X. Tang, X. Mao, C. Luo, M.-S. Wang, W.-Q. Deng and K.-L. Han, *J. Phys. Chem. Lett.*, 2018, 9, 3087–3092.
- 118 E. L. da Silva, J. M. Skelton, S. C. Parker and A. Walsh, *Phys. Rev. B: Condens. Matter Mater. Phys.*, 2015, **91**, 144107.
- 119 Z. Xiao, Y. Zhou, H. Hosono and T. Kamiya, *Phys. Chem. Chem. Phys.*, 2015, **17**, 18900–18903.

- 120 I. Chung, J.-H. Song, J. Im, J. Androulakis, C. D. Malliakas, H. Li, A. J. Freeman, J. T. Kenney and M. G. Kanatzidis, J. Am. Chem. Soc., 2012, 134, 8579–8587.
- 121 Y. Zhou, H. F. Garces, B. S. Senturk, A. L. Ortiz and N. P. Padture, *Mater. Lett.*, 2013, **110**, 127–129.
- 122 X. Qiu, B. Cao, S. Yuan, X. Chen, Z. Qiu, Y. Jiang, Q. Ye, H. Wang, H. Zeng, J. Liu and M. G. Kanatzidis, *Sol. Energy Mater. Sol. Cells*, 2017, **159**, 227–234.
- 123 A. G. Kontos, A. Kaltzoglou, E. Siranidi, D. Palles, G. K. Angeli, M. K. Arfanis, V. Psycharis, Y. S. Raptis, E. I. Kamitsos, P. N. Trikalitis, C. C. Stoumpos, M. G. Kanatzidis and P. Falaras, *Inorg. Chem.*, 2017, 56, 84–91.
- 124 T.-B. Song, T. Yokoyama, S. Aramaki and M. G. Kanatzidis, *ACS Energy Lett.*, 2017, 2, 897–903.
- 125 Y. Zong, Z. Zhou, M. Chen, N. P. Padture and Y. Zhou, *Adv. Energy Mater.*, 2018, **8**, 1800997.
- 126 Y. Zong, Y. Zhou, Y. Zhang, Z. Li, L. Zhang, M.-G. Ju, M. Chen, S. Pang, X. C. Zeng and N. P. Padture, *Chem*, 2018, 4, 1404–1415.
- 127 T. Liu, Y. Zhou, Z. Li, L. Zhang, M.-G. Ju, D. Luo, Y. Yang, M. Yang, D. H. Kim, W. Yang, N. P. Padture, M. C. Beard, X. C. Zeng, K. Zhu, Q. Gong and R. Zhu, Adv. Energy Mater., 2018, 8, 1800232.
- 128 A. Mura, I. Hideshima, Z. Liu, T. Hosoi, H. Watanabe and K. Arima, *J. Phys. Chem. C*, 2013, **117**, 165–171.
- 129 Z. Xiao, Y. Zhou, H. Hosono, T. Kamiya and N. P. Padture, *Chem. Eur. J.*, 2018, 24, 2305–2316.
- 130 M. Chen, M.-G. Ju, A. D. Carl, Y. Zong, R. L. Grimm, J. Gu, X. C. Zeng, Y. Zhou and N. P. Padture, *Joule*, 2018, 2, 558–570.
- 131 N. Sakai, A. A. Haghighirad, M. R. Filip, P. K. Nayak, S. Nayak, A. Ramadan, Z. Wang, F. Giustino and H. J. Snaith, J. Am. Chem. Soc., 2017, 139, 6030–6033.
- 132 B. A. Connor, L. Leppert, M. D. Smith, J. B. Neaton and H. I. Karunadasa, *J. Am. Chem. Soc.*, 2018, **140**, 5235–5240.
- 133 Z. Xiao, W. Meng, J. Wang and Y. Yan, *ChemSusChem*, 2016, 9, 2628–2633.
- 134 S. E. Creutz, E. N. Crites, M. C. De Siena and D. R. Gamelin, *Nano Lett.*, 2018, **18**, 1118–1123.
- 135 N.-K. Kim, Y. H. Min, S. Noh, E. Cho, G. Jeong, M. Joo, S.-W. Ahn, J. S. Lee, S. Kim, K. Ihm, H. Ahn, Y. Kang, H.-S. Lee and D. Kim, *Sci. Rep.*, 2017, 7, 4645.
- 136 H. Sternlicht, N. P. Padture and Y. Zhou, *Joule*, 2018, DOI: 10.1016/j.joule.2018.12.011.
- 137 G. Divitini, S. Cacovich, F. Matteocci, L. Cinà, A. Di Carlo and C. Ducati, *Nat. Energy*, 2016, **1**, 15012.
- 138 C. Liu, W. Li, J. Chen, J. Fan, Y. Mai and R. E. I. Schropp, Nano Energy, 2017, 41, 75–83.
- 139 S. Xiang, Z. Fu, W. Li, Y. Wei, J. Liu, H. Liu, L. Zhu, R. Zhang and H. Chen, ACS Energy Lett., 2018, 3, 1824–1831.